GLUT5 (*SLC2A5*) enables fructose-mediated proliferation independent of ketohexokinase

Roger J. Liang[1,2], Samuel Taylor[1,2,3,4], Navid Nahiyaan[5], Junho Song[2], Charles J. Murphy[6,7], Ezequiel Dantas[1], Shuyuan Cheng[3], Ting-Wei Hsu[3], Shakti Ramsamooj[1,2], Rahul Grover[8], Seo-Kyoung Hwang[1,2], Bryan Ngo[2,3], Lewis C. Cantley[2], Kyu Y. Rhee[5], and Marcus D. Goncalves[1,2]*

[1] Division of Endocrinology, Weill Department of Medicine, Weill Cornell Medicine, New York, NY 10065, USA

[2] Meyer Cancer Center, Department of Medicine, Weill Cornell Medicine, New York, NY 10065, USA

[3] Weill Cornell Graduate School of Medical Sciences, Weill Cornell Medicine, New York, NY 10065, USA

[4] Weill Cornell/Rockefeller/Sloan Kettering Tri-I MD-PhD program, New York, NY 10065, USA

[5] Division of Infectious Diseases, Weill Department of Medicine, Weill Cornell Medicine, New York, NY 10065, USA

[6] Center for Molecular Oncology, Memorial Sloan Kettering Cancer Center, New York, NY 10065, USA

[7] Department of Pathology, Memorial Sloan Kettering Cancer Center, New York, NY 10065, USA

[8] Weill Cornell Medical College, Weill Cornell Medicine, New York, NY 10065, USA

*Corresponding Author

Marcus D. Goncalves, MD, PhD

Assistant Professor of Medicine

Weill Cornell Medicine

413 E. 69th Street, Rm. 620

New York, NY 10021

Abstract:

Background: Fructose is an abundant source of carbon and energy for cells to use for metabolism, but only certain cell types use fructose to proliferate. Tumor cells that can metabolize fructose have a fitness advantage over their neighboring cells, but the proteins that mediate fructose metabolism in this context are unknown. Here, we investigated the determinants of fructose-mediated cell proliferation.

Methods: We quantified the ability of 14 cell lines to proliferate in fructose-containing media (i.e. the fructolytic ability) using live cell imaging and crystal violet assays. The expression and abundance of proteins related to fructose metabolism were assessed using RT-qPCR and western blot, respectively, for each cell line. Using a positive selection approach, we "trained" the non-fructolytic PC3 cell line to utilize fructose for proliferation. RNA-seq was then performed to identify key transcriptional changes associated with fructolytic ability. We overexpressed and deleted proteins associated with fructose metabolism, and performed metabolic profiling using the Seahorse Bioanalyzer and LC/MS-based metabolomics.

Results: We found that neither the tissue of origin nor expression level of any single gene related to fructose catabolism determine a cell's fructolytic ability. Cells cultured chronically in fructose can develop fructolytic ability if *SLC2A5,* encoding the fructose transporter, GLUT5, gets upregulated. Overexpression of GLUT5 in non-fructolytic cells enables growth in fructose-containing media across cells of different origins. GLUT5 permitted fructose to flux through glycolysis using hexokinase (HK) and not ketohexokinase (KHK).

Conclusions: We show that GLUT5 is a robust and generalizable driver of fructose-dependent cell proliferation. This indicates that fructose uptake is a limiting factor for fructose-mediated cell proliferation. We further demonstrate that cancer cell proliferation with fructose is independent of KHK.

Background:

Fructose is an important contributor to cell metabolism, growth, and disease. It is the second most abundant sugar in the blood and is commonly consumed as part of the Western diet. Most caloric sweeteners including sucrose, honey, and high fructose corn syrup contain at least 40% fructose, and the yearly consumption of these caloric sweeteners in the US is over 120 lbs (~60 kg) *per capita* (1). The excessive availability of fructose-containing sugars has negatively altered human physiology and predisposed us to cardiometabolic disease, insulin resistance, and obesity (2,3).

Fructose metabolism is tissue specific. Canonical fructose metabolizing organs include the kidney and those found in the gastrointestinal tract such as the liver, pancreas, and intestine. In these organs, fructose enters through the fructose transporter, GLUT5, before being phosphorylated by KHK and cleaved by Aldolase B (ALDOB) into glyceraldehyde and dihydroxyacetone phosphate. Both of the products can be metabolized into glyceraldehyde-3-phosphate, a downstream glycolytic intermediate. Digestive organs are directly exposed to dietary fructose on a daily basis, and they express high levels of fructose metabolism genes (4,5). Metabolic tracing experiments have proved that dietary fructose is metabolized to fructose-1-phosphate (F1P) in these organs (6). However, other organs—such as heart, muscle, and certain parts of the brain—have also been reported to metabolize fructose (5,7–11).

Tumors can also metabolize fructose. This has been shown for a variety of tumor types arising from the breast, brain, prostate, ovary, pancreas, intestine, lung, liver, kidney, and blood ((5,12), Breast: (13,14) Brain: (15,16), Prostate: (17), Ovary: Jin et al., 2019, Pancreas: (19,20), Intestine: (21), Lung: (22–24), Liver: (25), Kidney: (26), Blood:

(27,28)). In many of these cases, fructose has been shown to enter the cell through a membrane transporter, GLUT5, and then undergo metabolism into downstream glycolytic intermediates. In tumors, it has been presumed, but not clearly shown, that fructose is metabolized by ketohexokinase. It also remains unclear what basic machinery is required by tumor cells to permit fructose metabolism.

In this study, we set out to determine the cell-intrinsic factors that enable tumor cell proliferation in fructose. We profiled 13 cancer cell lines from 5 different origins and demonstrate that neither the tissue of origin nor expression level of any individual gene related to fructose metabolism determine fructolytic ability. We “trained” non-fructolytic cells in a high fructose, low glucose media in order to obtain cells that metabolize fructose. The trained cells showed strong upregulation in the expression of *SLC2A5*, the gene encoding GLUT5. Overexpression of GLUT5 allowed 6 non-fructolytic cell lines of different origins to proliferate in fructose media. This proliferation did not require KHK. Instead, fructose was preferentially metabolized by hexokinase. Taken together, these findings demonstrate that cells proliferate using fructose by upregulating GLUT5 independent of KHK.

Methods:

Experimental model and subject details

Cell culture

RKO, H508, HepG2, Huh7, HEK293T (293T), A172, U118-MG, U87, MCF-7, MDA-MB-468, and PC3 cells were obtained from ATCC. DLD1 and HCT116 cells were a generous gift from Lukas Dow. 22RV1 and was a generous gift from Dawid Nowak. 22Rv1, PC3, and H508 cells were cultured in full RPMI (Corning, Corning, NY) supplemented with 10% fetal bovine serum (FBS) (Gemini, Sacramento, CA) and 1% penicillin/streptomycin (Life Technologies, Carlsbad, CA). All of the other cells were cultured in DMEM (Corning) supplemented with 10% FBS and 1% penicillin/streptomycin (Life Technologies). HepG2 cells were grown on collagen coated plates (2 ug/cm^2). Cell lines were STR fingerprinted and/or bought from ATCC directly. Cells were tested for mycoplasma (Lonza, Basel, Switzerland).

Sugarless RPMI (Life Technologies) and DMEM (Life Technologies) were used in many experiments. Glucose (Millipore-Sigma, Burlington, MA) and fructose (St. Louis, MO) powders were diluted to 1 M stock in water before filtration. This stock solution was diluted into sugarless media.

To generate the semi-trained PC3 line, the parental cells were cultured in RPMI (Life Technologies) containing 1 mM glucose 10 mM fructose and 5% dFBS (Life Technologies). Cells were passaged approximately once per week. After >20 passages, semi-trained cells were cultured in 10 mM fructose in order to generate trained PC3 cells.

Method Details

RNA extraction, RT-qPCR, and RNA-seq

Total RNA was isolated directly from plates using the RNeasy Mini Kit (Qiagen, Hilden, Germany). For qPCR, 1.25 µg RNA was reversed transcribed using SuperScript VILO Master Mix (Thermo Fisher, Waltham, MA). Resulting cDNA was diluted 1:10 and qPCR was performed with Fast SYBR Green Mastermix (Life Technologies). The relative expression of each gene was calculated by comparative ΔCt method after normalizing to endogenous controls (Raw dCt in Table S2, Primers in Table S3). A heatmap of the results was produced using the Qlucore Omics Explorer (Qlucore, Lund, Sweden).

RNA samples from PC3 and semi-trained PC3 were submitted to the Weill Cornell Medicine Genomics Core for paired-end RNA-seq on a NovaSeq 6000. Raw sequenced reads were aligned to the mouse reference GRCm38 using STAR (v2.4.1d, 2-pass mode) aligner. Aligned reads were quantified using Cufflinks (v2.2.1) to obtain fragments per kilobase per million (FPKM). Statistical analyses on the normalized expression values (FPKM) were performed using the Qlucore Omics Explorer (Qlucore, Lund, Sweden). Gene expression levels were $\log_2$ transformed before performing PCA and differential gene expression analysis.

Genomic DNA (gDNA) extraction and qPCR

500 uL genomic lysis buffer (20 mM Tris-HCl pH 7.5, 20 mM EDTA, 1% SDS, 400 ug/mL proteinase K) was used to lyse 500,000 cells. Proteinase K was heat inactivated at 95°C for 15 minutes and allowed to cool to room temperature. Protein was

precipitated with 5 M NaCl, and sample was centrifuged at 13,000 x rpm at room temperature for 10 minutes. Supernatant was poured out and pellet was washed with 1 mL 70% ethanol. Samples were centrifuged for at 13,000 x rpm for 5 minutes and supernatant was drained. Pellets were resuspended in 10 mM Tris-HCl pH 8.0. To analyze *SLC2A5* copy number, qPCR was performed on 40 ng of gDNA using Fast SYBR Green Mastermix. Primers were designed to be within the same exon for *SLC2A5* and *B2M* and can be found in Table S3.

Cell line mutation and clinical data analysis

Cell line genomic data were downloaded from the Cancer Cell Line Encyclopedia (CCLE, Broad Institute) (29) or the COSMIC (Wellcome Sanger Institute) (30) databases and cross referenced with known oncogenic mutations from COSMIC tier 1 genes (Table S1). Full list of oncogenic mutations for each cell line can be found in Supplementary File 1. Mutation and clinical data for each cell line were cross referenced with Cellosaurus (Table S1) (31).

Cell confluence, viability, and the fructolytic index

Cells were plated at low confluency in a 6- or 12-well dish. After settling, cells received a PBS wash and were given 5% dFBS, 1% penicillin-streptomycin media containing no sugar, 10 mM glucose, or 10 mM fructose. Plates were loaded into IncuCyte ZOOM Live Cell Analysis System (Essen Bioscience, Ann Arbor, MI) for imaging. 16 frames per well were analyzed at each timepoint to determine confluency.

Change in confluency per hour was measured by linear regression on Prism (Graphpad, San Diego, CA).

Independent cell proliferation experiments were used to produce the fructolytic index (n = 3). It was calculated by dividing the relative growth in fructose (growth rate in fructose – growth rate in the no-sugar control) by the relative growth in glucose (growth rate in glucose – growth rate in the no-sugar control). After 3-4 days in the Incucyte system, cells were fixed with ice cold 80% methanol before. Crystal violet reagent (Sigma-Aldrich) was added to each well, and the plates were placed on a rocker for 30 minutes. Cells were then rinsed with water and imaged with a scanner.

For the competition assay, phase contrast and fluorescent images from the Incucyte system were exported as TIFF files. A custom ImageJ (Bethesda, MD) program (https://github.com/sam-taylor/CompCount) was used to acquire cell count and size. A bandpass filter, automatic threshold, and watershed algorithm were employed to distinguish cells from background. Data from the individual images were compiled into groups using MATLAB (Natick, MA) statistical software.

To measure sensitivity to drugs, cells were plated at low confluency with several replicates in a 96-well white bottom plate. The next day, powdered 2-DG (Sigma-Aldrich) was reconstituted in 10 mM glucose or 10 mM fructose media to make 100 mM 2-DG stock, which was then serially diluted. Cells were washed with PBS and were given 5% dFBS, 1% penicillin-streptomycin media containing either 100 µL of 10 mM glucose or 10 mM fructose media containing serially diluted 2-DG. Cell viability was measured after 72 hours using Cell Titer Glo reagent according to manufacturer's

158 instructions (Promega, Fitchburg, WI). Plates were covered and rocking for 15 minutes
159 before luminescence was measured.
160
161 **Western Blots**
162 Whole cell lysates were extracted with RIPA buffer (CST, Danvers, MA)
163 containing protease and phosphatase inhibitor (Life Technologies) and quantified with
164 BCA reagent (Thermo Fisher). Murine muscle, liver, and *Khk*$^{-/-}$ liver was obtained from
165 our previous study (21). Equal amounts of protein were diluted in 4x LDS buffer (Life
166 Technologies) before being run in 4-12% bis-tris gels (Invitrogen, Carlsbad, CA). Gels
167 were transferred to PVDF membranes (Perkin-Elmer, Waltham, MA) and blocked for 1
168 hour in 5% BSA in Tris-buffered saline containing .1% Tween 20 (TBST). Membranes
169 were probed while rocking at 4°C with the following antibodies and concentrations:
170 GLUT1 (Millipore 07-1401) 1:1000, GLUT2 (Abcam, Cambridge, UK, ab192599)
171 1:1000, GLUT5 (Invitrogen, PA5-80023) 1:1000, KHK (Abcam) 1:1000, HK1 (CST
172 2024) 1:1000, HK2 (CST 2867) 1:1000, ALDOA (CST8060) 1:1000, ALDOB (Abcam
173 ab152828) 1:1000, ALDOC (Proteintech, Rosemont, IL, 14884-1-AP) 1:1000, LDHA
174 (CST) 1:1000, LDHB (Abcam) 1:1000, GAPDH (Proteintech 10494-1-AP) 1:5000, Pan-
175 Actin (CST 4968) 1:1000, and V5-HRP (Life Technologies R96125) 1:5000. After
176 incubation, cells were washed with TBST before appropriate HRP-conjugated
177 secondary antibody was added for 1 hour. After 3 more TBST washes, membranes
178 were exposed to Supersignal West Dura (Life Technologies) and imaged using a
179 ChemiDoc MP Imaging System (BioRad, Hercules, CA).
180

Plasmids and cloning

The following plasmids were generously provided by researchers via Addgene: pSpCas9(BB)-2A-Puro (PX459) V2.0 (#62988) from Dr. Feng Zhang (Broad Institute) (Ran et al., 2013)m pDONR221-*SLC2A5* (#132090) from the RESOLUTE Consortium and Giuliu Superti-Furga (Research Center for Molecular Medicine of the Austrian Academy of Sciences), and pLenti-U6-tdTomato-P2A-BlasR (Lrt2B) (#110854) from Dr. Lukas Dow (Weill Cornell Medicine) (32).

We selected sgRNA (Figure S3) for human KHK at the beginning of exon 5 using CRISPRdirect (33). Oligonucleotide pairs were annealed and cloned into PX459 using BbsI-HF (New England Biolabs, Ipswich, MA) followed by a ligation reaction (New England Biolabs). PDONR221-GLUT5 was cloned according to Gateway Technology (Invitrogen) into pLenti7.3_V5_DEST (Invitrogen) using LR Clonase (Invitrogen) in order to generate pLenti7.3_V5_SLC2A5. These plasmids were generated in Stbl3 bacteria (Life Technologies) and were purified using Qiagen miniprep or maxiprep kits (Qiagen).

Generating knockouts

We plated 200,000 cells/well in a 6-well dish. The following day, cells were transfected with 3 µL Lipofectamine 2000 (Life Technologies) and 3 ug plasmid containing sgRNA in Optimem (Life Technologies)**.** The following day, media was changed. The day after media change, cells were selected with 2 ug/mL puromycin for 48 hours. 50 or 100 cells were then passaged into 10 cm dishes and were allowed to proliferate into visible colonies over 2 weeks. Single colonies with normal morphology

were selected using cloning cylinders (Thermo Fisher). Knockouts were verified by western blot and sanger sequencing.

Transduction

2,000,000 293T cells were plated in a 10-cm dish. The next day, cells were transfected with 30 µL Lipofectamine 2000, 9 ug psPAX2, 1 ug VSV-G, and 9 ug of either Lrt2b, pLenti7.3-V5 EV, pLenti7.3-V5-*SLC2A5.* Media was changed the following day. Viral particles were harvested 48 and 72 hours after initial media change. The 2 harvests were combined and aliquoted for storage in -80 C.

To generate PC3-red, parental cells were given 50% Lrt2b virus and 50% media as well as 10 ug/mL polybrene. The next day, cells were given 50% virus and 50% media as well as 10 ug/mL polybrene. Media was changed after 24 hours. The day after media change, cells were grown in media containing 10 ug/mL blasticidin (Invivogen, San Diego, CA). Overexpression was verified by microscopy.

To overexpress GLUT5, non-fructolytic cell lines from several origins were plated at low confluence in 6-well dishes. The next day, cells were given 50% EV or *SLC2A5* virus and 50% media as well as 10 ug/mL polybrene. Media was changed after 24 hours. Overexpression was verified by western blot.

Seahorse Assay

ECAR was measured with the Seahorse XFe96 Analyzer (Agilent, Santa Clara, CA), following manufacturer's Glycolytic Stress Test protocol. Briefly, 5,000 cells were plated in each well of a 96-well Seahorse assay plate. That same day, the assay

cartridge was hydrated and kept in a non-CO2 incubator at 37°C. After 12-24 hours, cells were washed with PBS before they were given reconstituted sugarless DMEM powder (Sigma-Aldrich) supplemented with 2 mM glutamine and 5 mM HEPES buffer. Cells were then incubated for 45 minutes at 37°C in a non-CO2 incubator. Compounds (final concentrations: Glucose 10 mM or fructose 10 mM, oligomycin 1 uM, and 2-DG 50 mM) were prepared, loaded into the flux pack, and put into the Seahorse XFe96 Analyzer. The plate containing cells were subsequently loaded into the machine. ECAR was analyzed using Seahorse Wave software.

Metabolite extraction, targeted analysis, and untargeted analysis

Metabolomics were carried out on cells to measure polar metabolites. 500,000 cells were plated in triplicate in 6-well dishes for each condition. The next day, cells were washed briefly with 37°C PBS before given media containing no glucose and 10 mM [U-^{13}C]-fructose (Cambridge Isotope Laboratories, Tewksbury, MA). After 30 minutes incubation, cells were washed briefly with warm PBS and immediately harvested into 2 mL Eppendorf tubes using with ice cold 80% methanol (Yuan et al., 2012) and 0.02 M formic acid. Cells were vortexed and stored in -80C overnight. Samples were spun down at 13,000 x RPM for 10 minutes at 4°C. Supernatant was transferred to a new Eppendorf tube and was evaporated for LC/MS.

Quantitative metabolomics were performed on samples as previously described (21). Briefly, 5 µL of each filtered extract was injected through an Agilent ZORBAX Extend C18, 2.1 x 150 mm, 1.8 (Agilent) downstream of an Agilent ZORBAX SB-C8, 2.1 mm x 30 mm, 3.5 um guard column (Agilent) heated to 40°C in the Agilent 1290 Infinity

LC system. Solvent A (97% water/ 3% methanol containing 5 mM tetrabutylammonium hydroxide (TBA) and 5.5 mM acetic acid) and Solvent B (methanol containing 5 mM TBA and 5.5 mM acetic acid) were infused at a 0.250 mL/min flow rate. The reverse phase gradient was as follows: 0-3.5 min, 0% B; 4-7.5 min, 30% B; 8-15 min, 35% B; 20-24 min, 99% B; followed by a 7-minute run at 0% B. Acquisition was performed on the Agilent 6230 TOF mass spectrometer (Agilent) using an Agilent Jet Stream electrospray ionization source (Agilent) operated at 4000 V Cap and 2000 V nozzle voltage in high resolution, negative mode. During acquisition, the sample nebulizer was set to 45 psig with sheath gas flow of 12L/min at 400°C. Drying gas was kept at 325°C at 8 L/min. The fragmentor was set to 125 V, with the skimmer set to 50 V and Octopole Vpp at 400 V. Samples were acquired in centroid mode for 1.5 spectra/s for m/z's from 50-1100.

Data was analyzed by batch processing with Agilent MassHunter Profinder software (Agilent) for both targeted and untargeted analysis. For targeted analysis, we identified metabolites by both retention time and with authentic standards. We identified untargeted compounds using Profinder Batch Targeted Feature Extraction. Then, we processed hits through Agilent Mass Profiler Professional software for quality control.

Quantification and statistical analysis

Sample size was estimated based on prior data (21). Data is presented as ± standard error of the mean (SEM), calculated by Graphpad Prism 8. For total metabolites and GLUT5 rescue growth rates, unpaired two-tail t tests were done between control and experimental conditions. For RT-qPCR data and 13C

metabolomics, two-way ANOVA was done with post-test comparisons made by Fisher's LSD test. Statistical significance is indicated in figures using the following denotation: *P < 0.05, **P< 0.01, ***P < 0.001, and ****P < 0.0001. Sample number was noted in figure legends.

Software availability

An application to perform cell quantification from images is created by S.T and available on https://github.com/sam-taylor/CompCount.

Results:

The fructolytic index quantifies proliferation using fructose relative to glucose

We measured the ability of 13 tumor cell lines to proliferate in 10 mM fructose and in 10 mM glucose using live cell imaging. Cells were sampled from a variety of organs including the brain, breast, prostate, liver, and colon/rectum. We noticed a striking difference in the ability of cells to proliferate in fructose as determined by live cell imaging (Figure S1A). For example, metastatic prostate PC3 cells do not grow in fructose media, but hepatocellular carcinoma HepG2 cells do (Figure 1A). We verified these results with a crystal violet assay after 3-4 days of growth (Figure S1B).

To quantify and compare the fructolytic ability among the cells, we created the fructolytic index. This index is calculated by dividing the relative growth in fructose (growth rate in fructose minus growth rate in the no-sugar control) by the relative growth in glucose (growth rate in glucose minus growth rate in the no-sugar control) (Figure S2A). In other words, it is a ratio of how well cells utilize fructose compared to glucose as a growth substrate (Figure 1B). Of note, we used 5% dialyzed FBS (dFBS) to minimize the contamination of FBS-related sugars to the media. The concentration of dFBS in the culture media was held constant at 5% in all cell lines except for 22RV1, which required 1% in our growth assays (Figure S2B-C).

Neither the tissue of origin nor expression level of any individual gene related to fructose metabolism determines fructolytic growth

There was heterogeneity in the fructolytic index amongst cells derived from the same tissue (Figure 1C). We reviewed the genomic mutations and clinical parameters

303 associated with each cell line and found no obvious trend that predicts fructose growth
304 (Table S1). We also profiled the cell lines for their expression of select fructolytic and
305 glycolytic genes and found no clear correlation of any individual transcript or protein with
306 the fructolytic index (Figure 1D-E, Table S2). Unbiased hierarchical clustering of the
307 samples according to gene expression similarly failed to group the cells by fructolytic
308 index (Figure S2D). Taken together, commonly used methods and existing bioinformatic
309 annotations failed to predict the fructolytic index of cell lines.
310
311 **Cells can be trained to proliferate with fructose**
312 To determine how cells utilize fructose, we attempted to "train" a non-fructolytic cell
313 line to proliferate using this sugar. We employed a positive selection approach that was
314 inspired by *in vitro* drug resistance studies, whereby researchers add selective pressure
315 to bacteria or tumor cells in order to find and characterize drug-resistant clones (34,35)
316 (Figure 2A). PC3, a cell line with a low fructolytic index, was grown in media containing
317 high fructose and limiting amounts of glucose for several passages. The original PC3 line
318 was cultured with non-fructose containing media in parallel as a control.
319 By passage 10 (P10), the line grown in fructose gained the ability to proliferate in
320 fructose, albeit only at high concentrations (>62.5mM) (Figure 2B). By passage 20 (P20),
321 the cells could proliferate at lower concentrations (>10mM) of fructose, and we called
322 these cells "semi-trained" (Figure S3A-B). We next removed glucose completely from
323 culture media of the "semi-trained" cell lines in hopes of selecting for cells that best
324 proliferated in fructose (Figure 2C). Recovered cells initially proliferated slowly, but after

1-2 passages, “trained” cells proliferated equally well in glucose and fructose (Figure 2D-E, Supplemental video 1).

To control for plating and media conditions, we co-plated the parental PC3 line with the trained cells in a competition assay (36) (Figure 2C). Parental cells were labeled with an RFP reporter and plated at a 1:1 ratio with trained cells. In glucose-media, the final number of parental and trained cells were equal, but in fructose-media, the parental cells only constituted 10-15% of total cells (Figure 2F, Supplemental Video 1-2). We next asked if the acquired ability to proliferate with fructose was lost when cells were grown in glucose for long periods of time. After 5 passages in glucose-media, the cells completely retained their fructolytic ability (Figure S3C-E).

GLUT5 mRNA and protein abundance correlates with fructolytic ability

We cultured the parental and semi-trained PC3 cells for either 24 or 48 hours in media containing either 11 mM glucose (full RPMI) or 1 mM glucose plus 10 mM fructose (Figure S4A). We then extracted RNA and performed next-generation sequencing to analyze expression across the transcriptome (RNA-seq) to capture intrinsic differences between the cells. Small differences in gene expression between the parental and semi-trained cells would presumably be enhanced in the trained cells.

The RNA-seq results were first summarized in a 3-dimensional principal components analysis (PCA), which revealed unique clusters separating the parental from semi-trained cells as well as the different media conditions (Figure S4B). Only fifteen genes were differentially expressed between the parental and semi-trained cells, even when using a generous statistical threshold (q=0.4 and $\log_2$ fold change>1.1), confirming

that the cells remained very similar despite being separated for > 20 passages (Figure 3A, Figure S4C). We validated the expression of these 15 genes together with several fructolytic and glycolytic enzymes using cDNA from parental, semi-trained, and trained cells (Figure 3B, S4D, S4F). From these data, we observed that the expression of *SLC2A5* had the highest fold change difference and correlated with fructolytic ability. There was a >30x fold increase in semi-trained cells and >200x increase in trained PC3 cells (Figure 3B). GLUT5 protein levels were also increased in trained PC3 cells compared to their parental PC3 cells (Figure 3C). We further showed that the increased level of GLUT5 expression was not due to an increase in *SLC2A5* copy number (Figure S4E).

GLUT5 overexpression rescues growth with fructose across cell lines of different origin independent of KHK

To test whether GLUT5 permits fructolytic growth in other cell lines, we overexpressed GLUT5 in brain, breast, prostate, colon, and liver cancer cell lines and repeated the proliferation assays. The overexpression of GLUT5 was sufficient to permit cellular proliferation in fructose without affecting expression of other fructolytic or glycolytic genes (Figure 3D, Figure S5A-C).

KHK has been described as a rate-limiting enzyme for fructose metabolism in tumor and normal tissue (9,15,37). To test whether KHK overexpression rescues fructose-mediated cell growth, we overexpressed KHK-A in non-fructolytic RKO cells and saw no rescue of cell proliferation (Figure S6A-B).

GLUT5 overexpression increases fructose flux into glycolysis

To measure differences in fructose metabolism between non-fructolytic and fructolytic cells, we cultured parental, semi-trained, and trained cells in media containing 10 mM [U-^{13}C]-fructose and traced its metabolic fate. The trained cells demonstrated increased levels of fructose-derived carbon into F1P, lactate, and TCA cycle intermediates (Figure 4A-B, Figure S7A-B). Measurable amounts of fructose were also detected in PC3 cells, suggesting that fructose can be imported into cells but does not meet the concentration necessary to sustain proliferation.

In order to gain real-time insight into the ability of fructose to acidify the media (presumably via lactate production), we measured the extracellular acidification rate (ECAR) using parental and trained PC3 cells (Figure 4C-D). While both cell types had similar ECAR in response to glucose, trained cells had much higher ECAR in response to fructose. Semi-trained cells showed an intermediate phenotype, as expected. Interestingly, 2-deoxyglucose (2-DG), a competitive inhibitor for HK, immediately extinguished both glucose- and fructose-induced ECAR. This led us to hypothesize that fructose flux to lactate is mediated by HK rather than the canonical fructose-metabolism protein, KHK.

Cells proliferate with fructose through hexokinase

Using CRISPR-Cas9, we generated a *KHK*$^{-/-}$ line using 293T cells (293T *KHK*$^{-/-}$) (Figure S8A-B). We then overexpressed either an empty vector (EV) or V5-tagged GLUT5 in the parental and *KHK*$^{-/-}$ cells (Figure S8C). The resulting cells were cultured in 10 mM [U-^{13}C]-fructose prior to recovery of polar metabolites for metabolomics. GLUT5

overexpression greatly increased the abundance of F1P and its proportion of fructose-derived carbons in the parental but not the *KHK*$^{-/-}$ cells (Figure S8D-E). However, the abundance and isotopic labeling patterns of lactate and TCA cycle intermediates were similar between GLUT5-overexpressing parental and *KHK*$^{-/-}$ cells (Figure S8D-E). Moreover, the absence of F1P did not affect cellular proliferation with fructose, as GLUT5 overexpression rescued fructose mediated proliferation in both the parental as well as the *KHK*$^{-/-}$ cells (Figure 4E). We therefore conclude that KHK is dispensable for fructose-mediated cell proliferation.

We capitalized on the kinetic properties of HK to discern whether fructose-mediated cell proliferation was mediated by KHK or HK. HK has a higher affinity for glucose than it does for fructose (38). Therefore, we hypothesized that if cells used KHK for growth, then they would be more resistant to the HK inhibitor, 2-DG, when cultured in fructose as compared to glucose. Alternatively, we hypothesized that if cells primarily used HK for growth, then they would be more sensitive to 2-DG when cultured in fructose as compared to glucose. We treated cells with increasing concentrations of 2-DG in media containing either 10 mM fructose or 10 mM glucose and found that cells in the fructose media were 5-33x more sensitive to 2-DG (Figure 4F). Taken together, we conclude that cells can adapt to metabolize fructose through upregulation of GLUT5 independent of KHK.

Discussion

Cells preferentially metabolize the nutrients available in their microenvironment. Transformed cells acquire the ability to metabolize novel nutrients which allow them to

outgrow their neighbors and survive in sites of metastasis. Understanding how tumor cells acquire this ability is valuable given the growing interest in metabolic and dietary interventions as anti-cancer therapy (39). Here, we show that human cancer cells from a wide range of origins can acquire the ability to metabolize fructose simply by stable overexpression of GLUT5. These data suggest that sugar uptake can be a limiting factor preventing fructose-mediated cell proliferation.

Sugar uptake is also a key regulatory node for glucose metabolism and growth. For example, the expression of the glucose transporters, GLUT1 and GLUT4, control skeletal muscle glucose uptake at rest and in response to contraction or insulin (40,41). Additionally, the expression of GLUT1 and GLUT3 in tumors is associated with enhanced glucose uptake and oncogenic growth (42–44). Tumor cells continue to regulate the flux of glucose at the levels of phosphorylation by HK, fructose-1,6- bisphosphate production by phosphofructokinase, and lactate export (45). In this study, we show that fructose phosphorylation by KHK is not required for fructose metabolism and cell growth; however, we speculate that other regulatory nodes exist.

Our conclusions are supported by clinical evidence from subjects with cancer. GLUT5 is significantly upregulated in tumors from patients with colon, lung, and breast adenocarcinoma, acute myeloid leukemia, ovarian carcinoma, and glioma where it contributes to malignancy and poor survival (16,21,23,25–27,27). Our data confirms that GLUT5 overexpression is sufficient to promote cellular proliferation in fructose, but the abundance of the GLUT5 transcript in our initial profiling did not predict the fructolytic index across cell lines. For example, H508 (fructolytic) and RKO (non-fructolytic) cells are from the same colorectal origin with similar levels of GLUT5 yet have vastly different

abilities to proliferate in fructose. Other groups have shown that the stability of GLUT5 mRNA and the location of GLUT5 protein can be modulated by distinct signaling pathways (5,46). Therefore, we conclude that GLUT5 expression needs to be analyzed in tandem with other, currently unknown, cellular features in order to determine fructose-mediated proliferation *a priori.*

Our data supports the conclusion that GLUT5 is a robust determinant of fructose-mediated cell proliferation. However, we were unable to identify how the semi-trained and trained cells upregulated this message. There was no difference in *SLC2A5* copy number in the genomic DNA and minimal change in the expression of known *SLC2A5*-regulating fructose-response elements like Chrebpβ (Figure 3, Figure S3). Due to the specificity of the *SLC2A5* overexpression, we hypothesize that the upregulation stems from epigenetic or genetic modifications at the *SLC2A5* locus.

Our data suggest that KHK is dispensable for fructose-mediated proliferation. Instead, we show that cancer cells metabolize fructose using HK, as is the case in lower order organisms. For example, *Hk* is the only fructokinase in yeast and the flux through HK sustains the high activity of nectarivore flight muscles (47,48). In humans, fructose is thought to be primarily metabolized by KHK, but this may be unique to non-proliferative cells in the liver, intestine, and kidney. Proliferating cells typically switch to less fructolytic isoforms of KHK. For example, liver cancer cells convert from the high affinity KHK-c variant (Km = 0.7 mM), to the low affinity isoform, KHK-a (Km = 7 mM), that may play a role in *de novo* nucleotide biosynthesis (49). On average, the cell lines we profiled in this study expressed >160x more KHK-a than KHK-c (Figure 1E, Table S1). Furthermore, the

462 expression of HK (Km = 1-4 mM) is even greater than KHK-a in these cells, which may
463 explain the preference for this route of metabolism (38,50).

464 The exact role of KHK and F1P in these cell lines remain unclear. KHK-mediated
465 fructose metabolism may become more important when HK is saturated or inhibited by
466 high concentrations of glucose and glucose 6-phosphate. However, it is unclear if glucose
467 ever reaches these high concentrations in poorly vascularized solid tumors (51). For
468 example, pancreatic adenocarcinomas in mice have significantly less glucose in the
469 tumor interstitial fluid relative to plasma (52). These poorly vascularized tumors also
470 receive less oxygen from the blood (51), and the resulting hypoxia enhances the
471 endogenous production of fructose and the expression of fructolytic genes (9,53–56).

472 In conclusion, our study defines fructose uptake as a limiting factor for fructose-
473 mediated cell proliferation. We describe a previously unappreciated role of HK to permit
474 fructolytic cell growth. These findings advance our basic understanding of fructose
475 metabolism in cancer cells and highlight a limitation of directly targeting KHK for anti-
476 cancer therapy.

477
478 **Conclusions**
479
480 The intent of this study was to find the determinants of fructose-mediated
481 proliferation in cell lines. We have found that fructose-dependent proliferation of cancer
482 cells is not determined by tissue of origin nor expression of any individual fructolytic gene.
483 Using a positive selection approach, we were able to train PC3 cells to proliferate with
484 fructose. We saw that GLUT5 was strongly upregulated in trained cells and that
485 overexpressing GLUT5 allowed non-fructolytic cell lines of several different origins to
486 proliferate in fructose. Lastly, we showed that cells metabolize fructose through

hexokinase, not ketohexokinase, to sustain proliferation and glycolysis. This study sheds light on cell-autonomous fructose metabolism and suggests that targeting fructose metabolism may require inhibition of both KHK as well as HK.

Key words: Fructose; ketohexokinase; hexokinase; GLUT5 (SLC2A5); metabolism

Abbreviations:

HK: Hexokinase

KHK: Ketohexokinase

ALDOB: Aldolase B

F1P: Fructose-1-phosphate

FBS: Fetal bovine serum

dFBS: dialyzed FBS

PCA: Principle components analysis

2-DG: 2-deoxyglucose

EV: empty vector

SEM: Standard error of the mean

References

1. United States Department of Agriculture, Economic Research Service. USDA Sugar Supply: Table 50: US Consumption of Caloric Sweeteners. 2019; Available from: https://www.ers.usda.gov/data-products/sugar-and-sweeteners-yearbook-tables/sugar-and-sweeteners-yearbook-tables/#World%20Production,%20Supply,%20and%20Distribution
2. Hannou SA, Haslam DE, McKeown NM, Herman MA. Fructose metabolism and metabolic disease. J Clin Invest. 2018 Feb 1;128(2):545–55.
3. Khitan Z, Kim DH. Fructose: A Key Factor in the Development of Metabolic Syndrome and Hypertension. J Nutr Metab [Internet]. 2013 [cited 2020 May 31];2013. Available from: https://www.ncbi.nlm.nih.gov/pmc/articles/PMC3677638/
4. Diggle CP, Shires M, Leitch D, Brooke D, Carr IM, Markham AF, et al. Ketohexokinase: expression and localization of the principal fructose-metabolizing enzyme. J Histochem Cytochem Off J Histochem Soc. 2009 Aug;57(8):763–74.
5. Douard V, Ferraris RP. Regulation of the fructose transporter GLUT5 in health and disease. Am J Physiol - Endocrinol Metab. 2008 Aug;295(2):E227–37.
6. Jang C, Hui S, Lu W, Cowan AJ, Morscher RJ, Lee G, et al. The Small Intestine Converts Dietary Fructose into Glucose and Organic Acids. Cell Metab. 2018 Feb;27(2):351-361.e3.
7. Funari VA, Herrera VLM, Freeman D, Tolan DR. Genes required for fructose metabolism are expressed in Purkinje cells in the cerebellum. Brain Res Mol Brain Res. 2005 Dec 14;142(2):115–22.

8. Funari VA, Crandall JE, Tolan DR. Fructose metabolism in the cerebellum. Cerebellum Lond Engl. 2007;6(2):130–40.
9. Mirtschink P, Krishnan J, Grimm F, Sarre A, Hörl M, Kayikci M, et al. HIF-driven SF3B1 induces KHK-C to enforce fructolysis and heart disease. Nature. 2015 Jun 25;522(7557):444–9.
10. Oppelt SA, Zhang W, Tolan DR. Specific regions of the brain are capable of fructose metabolism. Brain Res. 2017 15;1657:312–22.
11. Song (宋志林) Z, Roncal-Jimenez CA, Lanaspa-Garcia MA, Oppelt SA, Kuwabara M, Jensen T, et al. Role of fructose and fructokinase in acute dehydration-induced vasopressin gene expression and secretion in mice. J Neurophysiol. 2017 Feb 1;117(2):646–54.
12. Charrez B, Qiao L, Hebbard L. The role of fructose in metabolism and cancer. Horm Mol Biol Clin Investig. 2015 May 1;22(2):79–89.
13. Fan X, Liu H, Liu M, Wang Y, Qiu L, Cui Y. Increased utilization of fructose has a positive effect on the development of breast cancer. PeerJ. 2017;5:e3804.
14. Jiang Y, Pan Y, Rhea PR, Tan L, Gagea M, Cohen L, et al. A sucrose-enriched diet promotes tumorigenesis in mammary gland in part through the 12-lipoxygenase pathway. Cancer Res. 2016 Jan 1;76(1):24–9.
15. Gao W, Li N, Li Z, Xu J, Su C. Ketohexokinase is involved in fructose utilization and promotes tumor progression in glioma. Biochem Biophys Res Commun. 2018 10;503(3):1298–306.
16. Su C, Li H, Gao W. GLUT5 increases fructose utilization and promotes tumor progression in glioma. Biochem Biophys Res Commun. 2018 02;500(2):462–9.

17. Carreño D, Corro N, Torres-Estay V, Véliz LP, Jaimovich R, Cisternas P, et al. Fructose and prostate cancer: toward an integrated view of cancer cell metabolism. Prostate Cancer Prostatic Dis. 2019;22(1):49–58.
18. Jin C, Gong X, Shang Y. GLUT5 increases fructose utilization in ovarian cancer. OncoTargets Ther. 2019 Jul 8;12:5425–36.
19. Hsieh C-C, Shyr Y-M, Liao W-Y, Chen T-H, Wang S-E, Lu P-C, et al. Elevation of β-galactoside α2,6-sialyltransferase 1 in a fructose-responsive manner promotes pancreatic cancer metastasis. Oncotarget. 2016 Dec 9;8(5):7691–709.
20. Liu H, Huang D, McArthur DL, Boros LG, Nissen N, Heaney AP. Fructose induces transketolase flux to promote pancreatic cancer growth. Cancer Res. 2010 Aug 1;70(15):6368–76.
21. Goncalves MD, Lu C, Tutnauer J, Hartman TE, Hwang S-K, Murphy CJ, et al. High-fructose corn syrup enhances intestinal tumor growth in mice. Science. 2019 Mar 22;363(6433):1345–9.
22. Chen W-L, Jin X, Wang M, Liu D, Luo Q, Tian H, et al. GLUT5-mediated fructose utilization drives lung cancer growth by stimulating fatty acid synthesis and AMPK/mTORC1 signaling. JCI Insight. 2020 Feb 13;5(3).
23. Weng Y, Zhu J, Chen Z, Fu J, Zhang F. Fructose fuels lung adenocarcinoma through GLUT5. Cell Death Dis [Internet]. 2018 May 10 [cited 2020 May 24];9(5). Available from: https://www.ncbi.nlm.nih.gov/pmc/articles/PMC5945656/
24. Weng Y, Fan X, Bai Y, Wang S, Huang H, Yang H, et al. SLC2A5 promotes lung adenocarcinoma cell growth and metastasis by enhancing fructose utilization. Cell Death Discov. 2018 Dec;4:38.

25. Bu P, Chen K-Y, Xiang K, Johnson C, Crown SB, Rakhilin N, et al. Aldolase B Mediated Fructose Metabolism Drives Metabolic Reprogramming of Colon Cancer Liver Metastasis. Cell Metab. 2018 Jun 5;27(6):1249-1262.e4.
26. Jin X, Liang Y, Liu D, Luo Q, Cai L, Wu J, et al. An essential role for GLUT5-mediated fructose utilization in exacerbating the malignancy of clear cell renal cell carcinoma. Cell Biol Toxicol. 2019;35(5):471–83.
27. Chen W-L, Wang Y-Y, Zhao A, Xia L, Xie G, Su M, et al. Enhanced Fructose Utilization Mediated by SLC2A5 Is a Unique Metabolic Feature of Acute Myeloid Leukemia with Therapeutic Potential. Cancer Cell. 2016 Nov 14;30(5):779–91.
28. Zhao P, Huang J, Zhang D, Zhang D, Wang F, Qu Y, et al. SLC2A5 overexpression in childhood philadelphia chromosome-positive acute lymphoblastic leukaemia. Br J Haematol. 2018;183(2):242–50.
29. Barretina J, Caponigro G, Stransky N, Venkatesan K, Margolin AA, Kim S, et al. The Cancer Cell Line Encyclopedia enables predictive modelling of anticancer drug sensitivity. Nature. 2012 Mar;483(7391):603–7.
30. Tate JG, Bamford S, Jubb HC, Sondka Z, Beare DM, Bindal N, et al. COSMIC: the Catalogue Of Somatic Mutations In Cancer. Nucleic Acids Res. 2019 Jan 8;47(Database issue):D941–7.
31. Bairoch A. The Cellosaurus, a Cell-Line Knowledge Resource. J Biomol Tech JBT. 2018 Jul;29(2):25–38.
32. Zafra MP, Schatoff EM, Katti A, Foronda M, Breinig M, Schweitzer AY, et al. Optimized base editors enable efficient editing in cells, organoids and mice. Nat Biotechnol. 2018;36(9):888–93.

33. Naito Y, Hino K, Bono H, Ui-Tei K. CRISPRdirect: software for designing CRISPR/Cas guide RNA with reduced off-target sites. Bioinformatics. 2015 Apr 1;31(7):1120–3.
34. Rosa R, Monteleone F, Zambrano N, Bianco R. In Vitro and In Vivo Models for Analysis of Resistance to Anticancer Molecular Therapies. Curr Med Chem. 2014 May;21(14):1595–606.
35. Yudkin J. Origin of Acquired Drug Resistance in Bacteria. Nature. 1953 Mar;171(4352):541–6.
36. Eekels JJM, Pasternak AO, Schut AM, Geerts D, Jeeninga RE, Berkhout B. A competitive cell growth assay for the detection of subtle effects of gene transduction on cell proliferation. Gene Ther. 2012 Nov;19(11):1058–64.
37. Ishimoto T, Lanaspa MA, Le MT, Garcia GE, Diggle CP, MacLean PS, et al. Opposing effects of fructokinase C and A isoforms on fructose-induced metabolic syndrome in mice. Proc Natl Acad Sci U S A. 2012 Mar 13;109(11):4320–5.
38. Cárdenas ML, Rabajille E, Niemeyer H. Fructose is a good substrate for rat liver “glucokinase” (hexokinase D). Biochem J. 1984 Sep 1;222(2):363–70.
39. Lien EC, Vander Heiden MG. A framework for examining how diet impacts tumour metabolism. Nat Rev Cancer. 2019 Nov;19(11):651–61.
40. Hansen PA, Gulve EA, Marshall BA, Gao J, Pessin JE, Holloszy JO, et al. Skeletal Muscle Glucose Transport and Metabolism Are Enhanced in Transgenic Mice Overexpressing the Glut4 Glucose Transporter. J Biol Chem. 1995 Jan 27;270(4):1679–84.

41. Ren JM, Marshall BA, Gulve EA, Gao J, Johnson DW, Holloszy JO, et al. Evidence from transgenic mice that glucose transport is rate-limiting for glycogen deposition and glycolysis in skeletal muscle. J Biol Chem. 1993 Aug 5;268(22):16113–5.
42. Birsoy K, Possemato R, Lorbeer FK, Bayraktar EC, Thiru P, Yucel B, et al. Metabolic determinants of cancer cell sensitivity to glucose limitation and biguanides. Nature. 2014 Apr 3;508(7494):108–12.
43. Onodera Y, Nam J-M, Bissell MJ. Increased sugar uptake promotes oncogenesis via EPAC/RAP1 and O-GlcNAc pathways. J Clin Invest. 2014 Jan 2;124(1):367–84.
44. Yun J, Rago C, Cheong I, Pagliarini R, Angenendt P, Rajagopalan H, et al. Glucose Deprivation Contributes to the Development of KRAS Pathway Mutations in Tumor Cells. Science. 2009 Sep 18;325(5947):1555–9.
45. Tanner LB, Goglia AG, Wei MH, Sehgal T, Parsons LR, Park JO, et al. Four key steps control glycolytic flux in mammalian cells. Cell Syst. 2018 Jul 25;7(1):49-62.e8.
46. Gouyon F, Caillaud L, Carriere V, Klein C, Dalet V, Citadelle D, et al. Simple-sugar meals target GLUT2 at enterocyte apical membranes to improve sugar absorption: a study in GLUT2-null mice. J Physiol. 2003 Nov 1;552(Pt 3):823–32.
47. Emmerich W, Radler F. The Anaerobic Metabolism of Glucose and Fructose by Saccharomyces bailii. Microbiology,. 1983;129(11):3311–8.
48. Welch KC, Chen CCW. Sugar flux through the flight muscles of hovering vertebrate nectarivores: a review. J Comp Physiol [B]. 2014 Dec;184(8):945–59.

640 49. Li X, Qian X, Peng L-X, Jiang Y, Hawke DH, Zheng Y, et al. A splicing switch from
641 ketohexokinase-C to ketohexokinase-A drives hepatocellular carcinoma formation.
642 Nat Cell Biol. 2016;18(5):561–71.
643 50. Grossbard L, Schimke RT. PURIFICATION AND COMPARISON OF SOLUBLE
644 FORMS. 1966;16.
645 51. Vaupel P. Tumor microenvironmental physiology and its implications for radiation
646 oncology. Semin Radiat Oncol. 2004 Jul 1;14(3):198–206.
647 52. Sullivan MR, Danai LV, Lewis CA, Chan SH, Gui DY, Kunchok T, et al.
648 Quantification of microenvironmental metabolites in murine cancers reveals
649 determinants of tumor nutrient availability. DeBerardinis R, van Lohuizen M,
650 DeBerardinis R, Frezza C, editors. eLife. 2019 Apr 16;8:e44235.
651 53. Andres-Hernando A, Johnson RJ, Lanaspa MA. Endogenous fructose production:
652 what do we know and how relevant is it? Curr Opin Clin Nutr Metab Care.
653 2019;22(4):289–94.
654 54. Armitage EG, Kotze HL, Allwood JW, Dunn WB, Goodacre R, Williams KJ.
655 Metabolic profiling reveals potential metabolic markers associated with Hypoxia
656 Inducible Factor-mediated signalling in hypoxic cancer cells. Sci Rep. 2015 Oct
657 28;5(1):15649.
658 55. Hamann I, Krys D, Glubrecht D, Bouvet V, Marshall A, Vos L, et al. Expression and
659 function of hexose transporters GLUT1, GLUT2, and GLUT5 in breast cancer—
660 effects of hypoxia. FASEB J. 2018 Apr 13;32(9):5104–18.
661 56. Kucharzewska P, Christianson HC, Belting M. Global Profiling of Metabolic
662 Adaptation to Hypoxic Stress in Human Glioblastoma Cells. PLoS ONE [Internet].

2015 Jan 29 [cited 2020 Jun 10];10(1). Available from:
https://www.ncbi.nlm.nih.gov/pmc/articles/PMC4310608/

Acknowledgements:

We would like to thank all members of the Goncalves Lab and the Cantley Lab, especially Drs. Ted Kastenhuber and Andrés Quieroz, for thoughtful discussion and advice. The R25 AI140472 provided educational resources for metabolomics. We would like to thank Dr. Feng Zhang (Broad Institute) for pSpCas9(BB)-2A-Puro (PX459) V2.0. The pDONR221_SLC2A5 plasmid was a gift from RESOLUTE Consortium & Giulio Superti-Furga. pLenti-U6-tdTomato-P2A-BlasR (LRT2B) was a gift from Lukas Dow. We would like to thank Weill Cornell Medicine Genomics Core for conducting RNA-seq.

Funding:

This work was supported by NIH R35 CA197588 (L.C.C.), NIH/NIAID R25 AI 140472 (K.Y.R), SU2C-AACR-DT22-17 (L.C.C.), NIH K08 CA230318 (M.D.G.), and NIH P50 CA211024 (M.D.G.). B.N. is supported by a National Science Foundation (NSF) Graduate Research Fellowship and a National Cancer Institute (NCI) of the National Institutes of Health (NIH) under the F99/K00 Career Transition Fellowship (F99CA234950).

Author contributions:

Conceptualization: R.J.L and M.D.G.; Methodology: R.J.L., S.T., L.C.C., K.Y.R., and M.D.G.; Investigation: R.J.L., S.T., N.N., C.J.M., E.D., S.C., T.H., S.R., R.G., S.H., B.N.; Formal analysis: R.J.L. and E.D.; Data curation: R.J.L. and J.S.; Visualization: R.J.L. and

M.D.G.; Investigation and validation: M.D.G.; Software: S.T., C.J.M, and J.S.; Supervision: L.C.C., K.Y.R., and M.D.G.; Writing, review, and editing: R.J.L. and M.D.G.; Resources: L.C.C., K.Y.R., and M.D.G.; Funding acquisition: L.C.C., K.Y.R., and M.D.G.

Competing interests:

L.C.C. is a founder and member of the board of directors of Agios Pharmaceuticals and is a founder and receives research support from Petra Pharmaceuticals. M.D.G. reports personal fees from Novartis, Petra Pharmaceuticals, and Bayer. He receives research support from Pfizer. L.C.C. and M.D.G. are inventors on patents (pending) for Combination Therapy for PI3K-associated Disease or Disorder, The Identification of Therapeutic Interventions to Improve Response to PI3K Inhibitors for Cancer Treatment, and Anti-Fructose Therapy for Colorectal and Small Intestine Cancers. L.C.C. and M.D.G. are co-founders and shareholders in Faeth Therapeutics. All other authors report no competing interests.

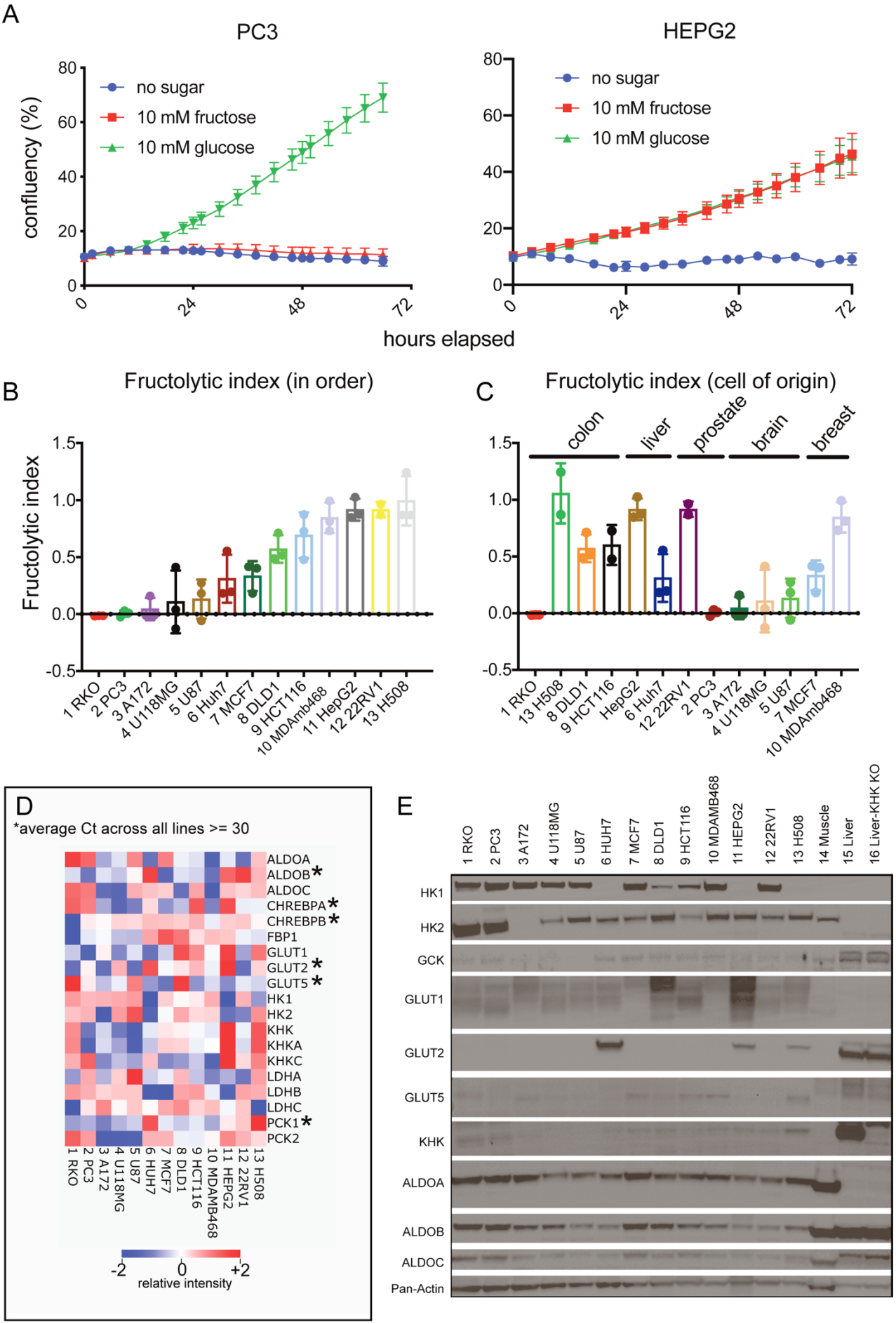
A
PC3
HEPG2
confluency (%)
no sugar
10 mM fructose
10 mM glucose
hours elapsed
B
Fructolytic index (in order)
Fructolytic index
1 RKO
2 PC3
3 A172
4 U118MG
5 U87
6 Huh7
7 MCF7
8 DLD1
9 HCT116
10 MDAmb468
11 HepG2
12 22RV1
13 H508
C
Fructolytic index (cell of origin)
colon
liver
prostate
brain
breast
D
*average Ct across all lines >= 30
ALDOA
ALDOB*
ALDOC
CHREBPA*
CHREBPB*
FBP1
GLUT1
GLUT2*
GLUT5*
HK1
HK2
KHK
KHKA
KHKC
LDHA
LDHB
LDHC
PCK1*
PCK2
relative intensity
E
HK1
HK2
GCK
GLUT1
GLUT2
GLUT5
KHK
ALDOA
ALDOB
ALDOC
Pan-Actin
14 Muscle
15 Liver
16 Liver-KHK KO

Figure 1

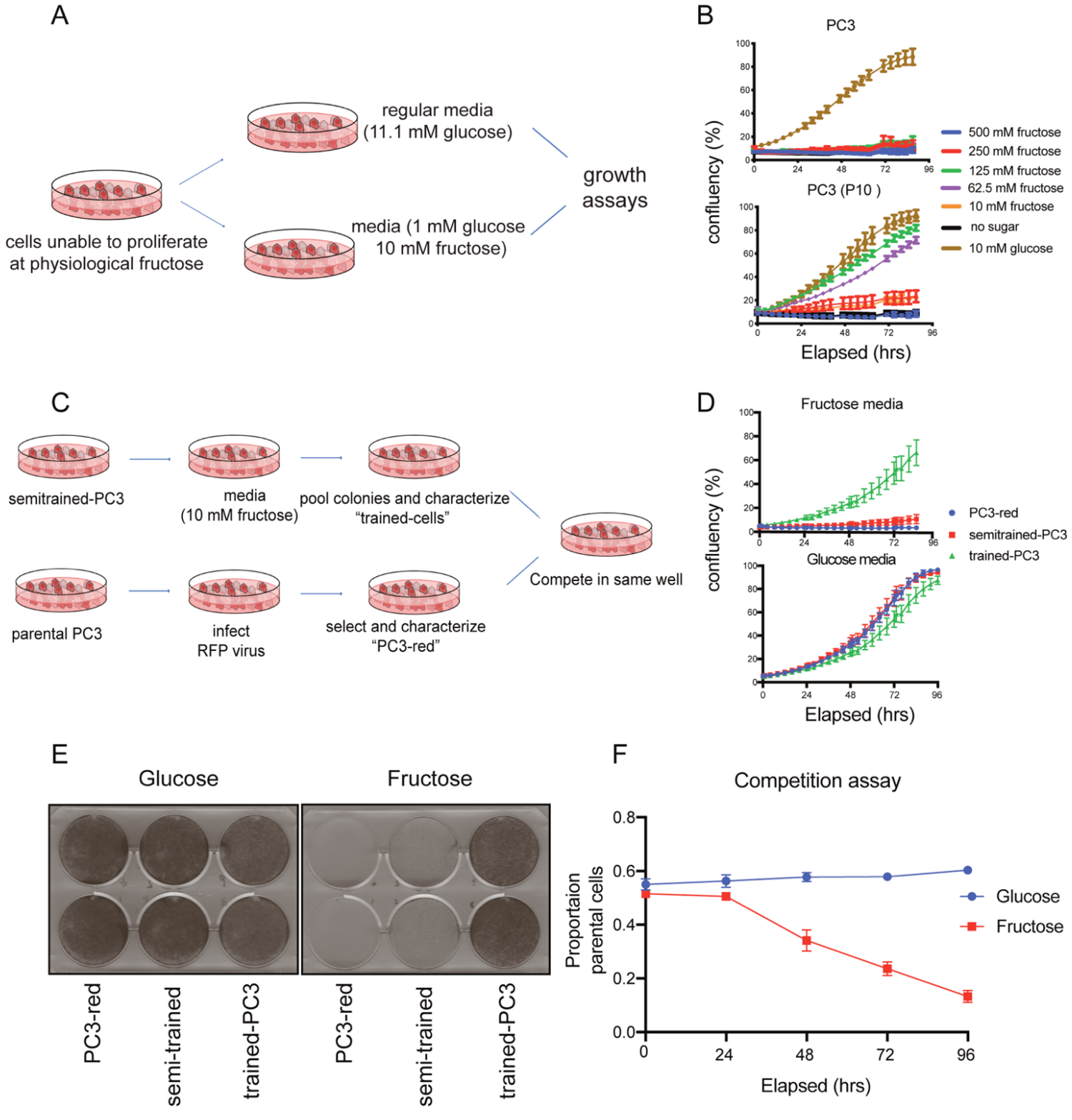
A
regular media
(11.1 mM glucose)
cells unable to proliferate
at physiological fructose
media (1 mM glucose
10 mM fructose)
growth
assays
B
PC3
confluency (%)
PC3 (P10)
Elapsed (hrs)
500 mM fructose
250 mM fructose
125 mM fructose
62.5 mM fructose
10 mM fructose
no sugar
10 mM glucose
C
semitrained-PC3
media
(10 mM fructose)
pool colonies and characterize
"trained-cells"
parental PC3
infect
RFP virus
select and characterize
"PC3-red"
Compete in same well
D
Fructose media
confluency (%)
Glucose media
Elapsed (hrs)
PC3-red
semitrained-PC3
trained-PC3
E
Glucose
Fructose
PC3-red
semi-trained
trained-PC3
PC3-red
semi-trained
trained-PC3
F
Competition assay
Proportaion
parental cells
Elapsed (hrs)
Glucose
Fructose

Figure 2

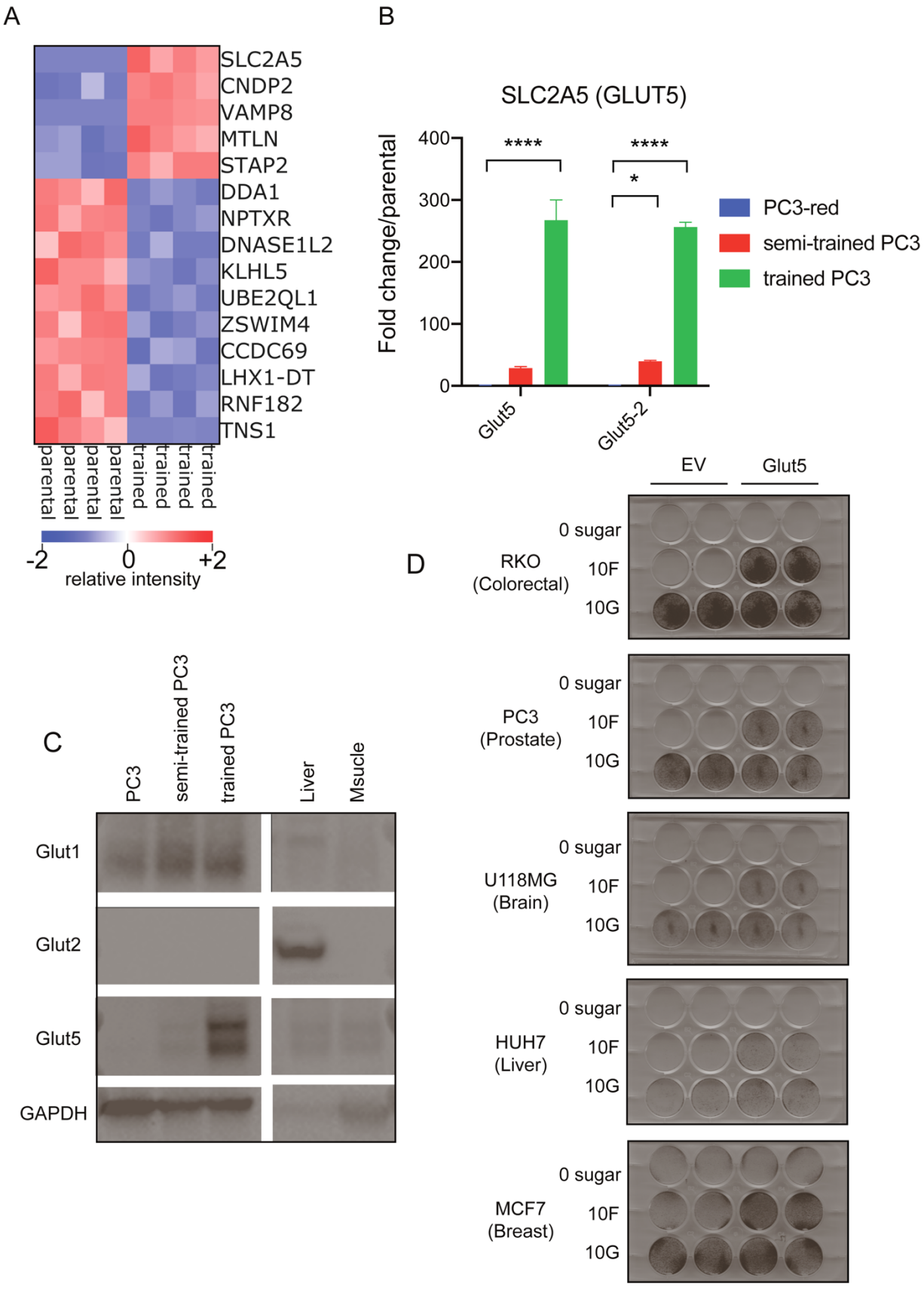
A
SLC2A5
CNDP2
VAMP8
MTLN
STAP2
DDA1
NPTXR
DNASE1L2
KLHL5
UBE2QL1
ZSWIM4
CCDC69
LHX1-DT
RNF182
TNS1
parental
parental
parental
parental
trained
trained
trained
trained
-2
0
+2
relative intensity
B
SLC2A5 (GLUT5)
Fold change/parental
400
300
200
100
0
****
****
*
Glut5
Glut5-2
PC3-red
semi-trained PC3
trained PC3
C
PC3
semi-trained PC3
trained PC3
Liver
Msucle
Glut1
Glut2
Glut5
GAPDH
D
EV
Glut5
RKO
(Colorectal)
PC3
(Prostate)
U118MG
(Brain)
HUH7
(Liver)
MCF7
(Breast)
0 sugar
10F
10G

Figure 3

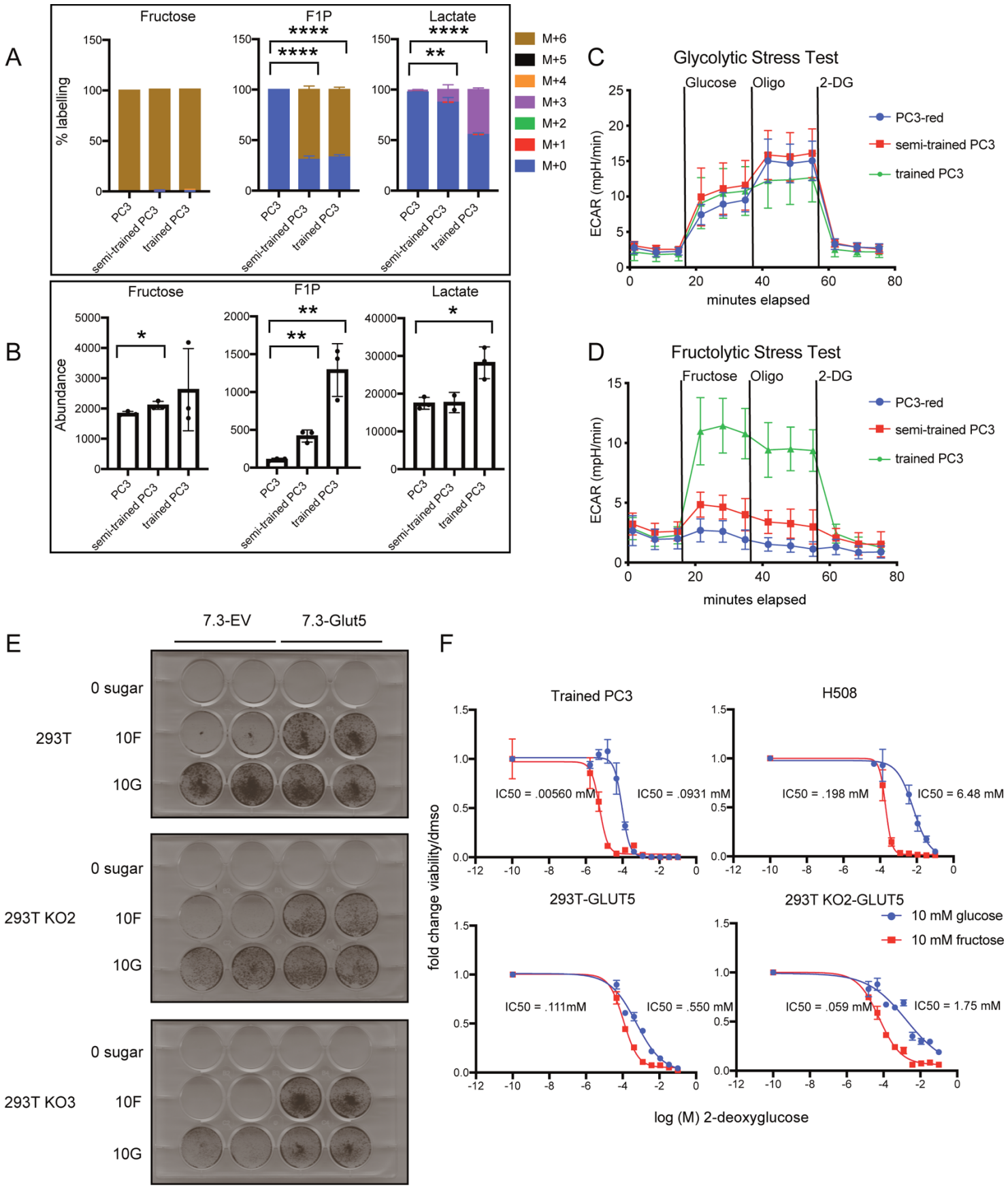
A
Fructose
F1P
Lactate
% labelling
M+6
M+5
M+4
M+3
M+2
M+1
M+0
PC3
semi-trained PC3
trained PC3
B
Abundance
C
Glycolytic Stress Test
Glucose
Oligo
2-DG
ECAR (mpH/min)
minutes elapsed
PC3-red
semi-trained PC3
trained PC3
D
Fructolytic Stress Test
E
7.3-EV
7.3-Glut5
293T
293T KO2
293T KO3
0 sugar
10F
10G
F
Trained PC3
H508
293T-GLUT5
293T KO2-GLUT5
IC50 = .00560 mM
IC50 = .0931 mM
IC50 = .198 mM
IC50 = 6.48 mM
IC50 = .111mM
IC50 = .550 mM
IC50 = .059 mM
IC50 = 1.75 mM
10 mM glucose
10 mM fructose
fold change viability/dmso
log (M) 2-deoxyglucose

Figure 4

Figure 1: Cellular gene expression and tissue of origin do not determine cellular proliferation in fructose.

(A) PC3 and HepG2 were seeded into 12-well plates (20,000 cells/well) and cultured in the absence or presence of 10 mM fructose, or 10 mM glucose media for approximately 3 days. Cell density (% confluency) was monitored over time using live cell imaging (n = 2 per media condition).
(B) Fructolytic index (fructose-mediated growth/glucose-mediated growth) of the indicated cell lines arranged in order of least to most fructolytic (n = 3).
(C) Fructolytic index of cell lines in (B) grouped by tissue of origin.
(D) Normalized expression of the indicated genes for each cell line shown as a heatmap. Cell lines ordered by fructolytic index (n = 2 per gene per cell line). * denotes $C_t > 30$.
(E) Immunoblot of the indicated proteins using lysates from the indicated cell lines, ordered from least to most fructolytic. Murine muscle, liver, and *Khk* knockout liver were used as controls.

Figure 2: Cells can be trained to metabolize fructose for proliferation

(A) Schematic for the positive selection strategy to generate fructolytic cell lines.
(B) PC3 and PC3 passage 10 (P10) cells were seeded into 96-well plate (1,500 cells/well) and cultured in media containing various amounts of sugar. Cell density (% confluency) was monitored over time using live cell imaging (n = 2 per condition).
(C) Schematic for the competition growth assay between PC3-red (parental PC3 cells transduced with RFP reporter) and fructose-trained cell lines.
(D) 40,000 of PC3, semi-trained PC3 passage 20 (P20), and trained-PC3 cells in 10 mM fructose or 11 mM glucose over time (n = 2 per condition).
(E) Cells from (D) were grown in 10 mM fructose or 11 mM glucose for 96 hours. They were then fixed and stained with crystal violet solution (n = 2 per condition).
(F) 20,000 PC3-red and 20,000 trained PC3 cells were seeded in the same well and cultured for 96 hours in 10 mM fructose or 10 mM glucose-containing media. Live fluorescent imaging was performed and the proportion of PC3-red cells to total PC3 cells is shown over time (n = 2 per condition). Supplemental Video 1 and Supplemental Video 2 are of competition assays monitored with live cell imaging.

Figure 3: GLUT5 overexpression rescues cellular proliferation in fructose

(A) Normalized expression of genes that are differentially expressed (q = 0.4, >1.1 $\log_2$ fold change) between PC3 and semi-trained PC3 cells (passage 20) presented in heatmap form.
(B) Relative expression of *SLC2A5* transcript in semi-trained PC3 and trained PC3 cells as compared to the parental PC3 line. Two primer sets were used. (n = 2 per condition). Two-way ANOVA with Fisher's LDS test. *P < 0.05, ****P < 0.0001
(C) Immunoblot of the indicated proteins using lysates from PC3, semi-trained PC3, and trained PC3 cells. Murine liver and muscle used as controls.
(D) GLUT5 or an empty vector (EV) were overexpressed in the indicated cells lines. The cells were plated at 20,000-30,000 cells/well and then grown in the presence of no sugar, 10 mM fructose, or 10 mM glucose. After 3 days, the cells were fixed and stained with crystal violet solution (n = 2 per condition).

Figure 4: Fructose fluxes through HK, not KHK, in order to sustain cellular proliferation

(A) Percent of heavy isotope (^{13}C) incorporation into fructose, fructose 1-phosphate (F1P), and lactate as detected by LC/MS from polar extracts of PC3, semi-trained PC3, and trained PC3 cells. (n = 2-3). The isotopic labelling is indicated by M+# designation indicated in the legend where the # represents the amount of [^{12}C] replaced by [^{13}C]. Two-tailed unpaired t tests were used between

parental and trained cells (M+3 for lactate, M+6 for fructose/F1P). *P < 0.05, **P< 0.01, and ****P < 0.0001.

(B) Total abundance of fructose, F1P, and lactate as detected by LC/MS from polar extracts of PC3, semi-trained PC3, and trained PC3 cells. (n = 2-3). Two-tailed unpaired t tests were used between parental and trained cells. *P < 0.05, **P< 0.01, and ****P < 0.0001.

(C) Extracellular acidification rate (ECAR) over time of PC3, semi-trained PC3, and trained PC3 cells under basal conditions and following the addition of glucose, oligomycin (Oligo), and 2-deoxyglucose (2-DG) at the indicated times. Data are the mean and SEM from 6 replicates.

(D) ECAR over time of PC3, semi-trained PC3, and trained PC3 cells under basal conditions and following the addition of fructose, Oligo, and 2-DG at the indicated times. Data are the mean and SEM from 6 replicates.

(E) GLUT5 or an empty vector (EV) were overexpressed in 293T or 293T *KHK* -/- cells. The cells were plated at 20,000 cells/well and then grown in the presence of no sugar, 10 mM fructose, or 10 mM glucose. After 7 days, the cells were fixed, stained with crystal violet solution (n = 2 per condition).

(F) Fold change in cell viability as assessed by ATP concentration (Cell Titer Glo) of the indicated fructolytic cell lines grown in either 10 mM glucose or 10 mM fructose containing the specified concentrations of 2-DG after 72 hours. (n = 3 per concentration). The half maximal inhibitory concentration (IC50) is displayed on the graph for each curve.

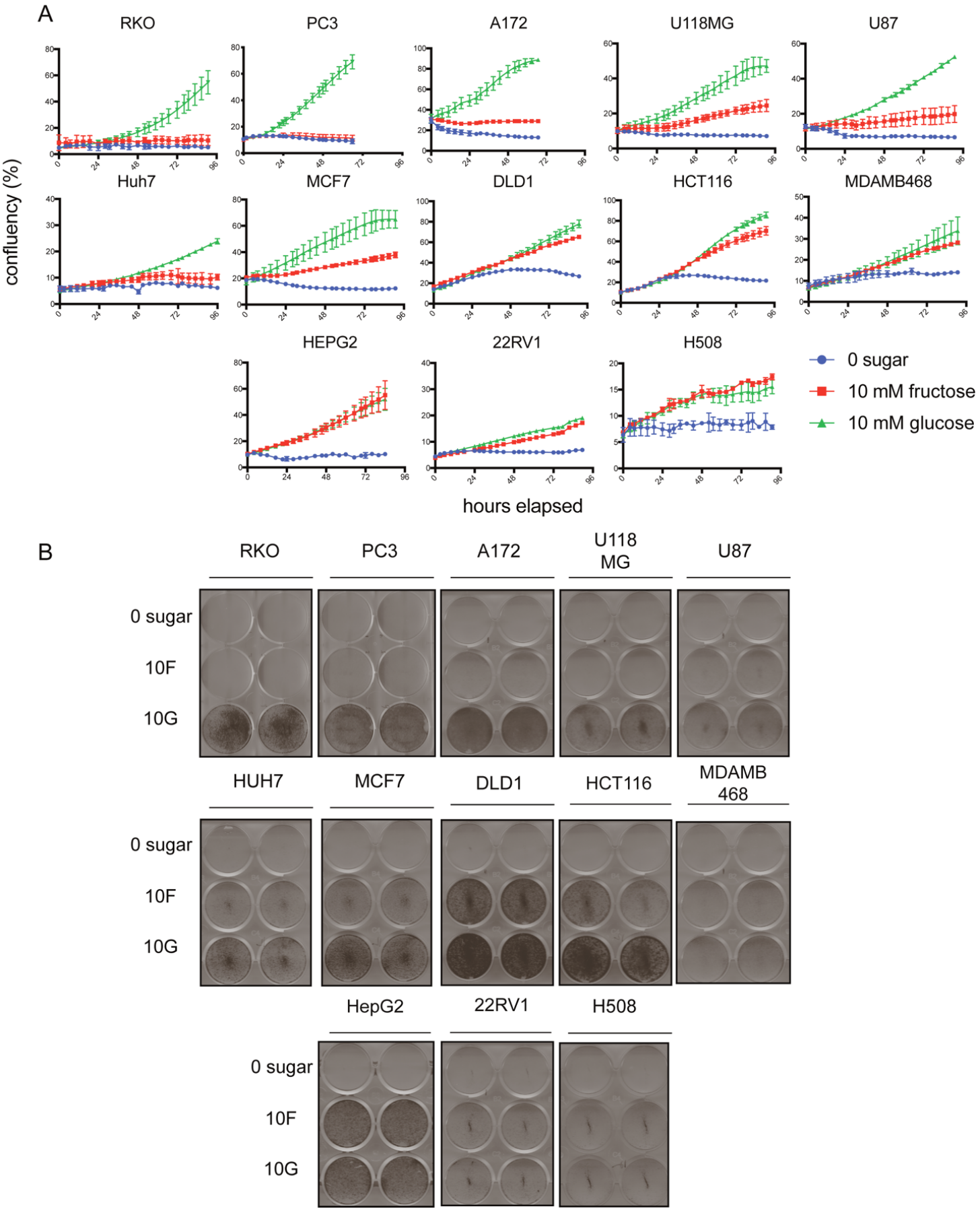

Supplemental Figure 1

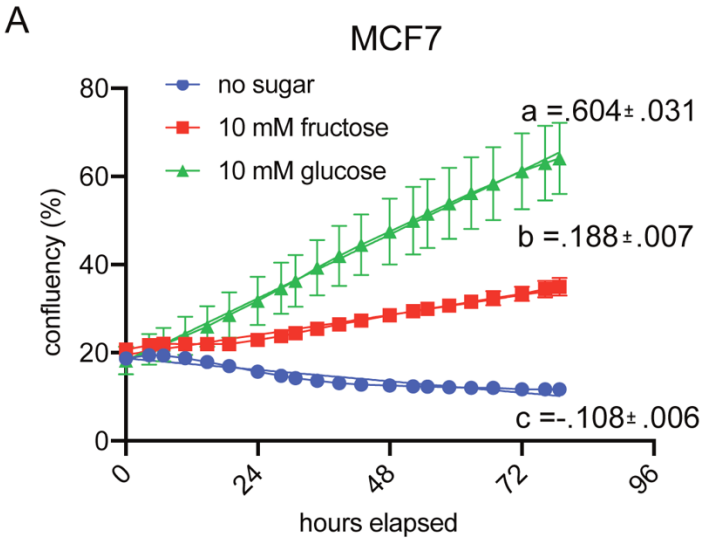

Fructolytic index = (b-c)/(a-c) = (.296 ± .013)/(.711 ± .037) = .416 ± .028

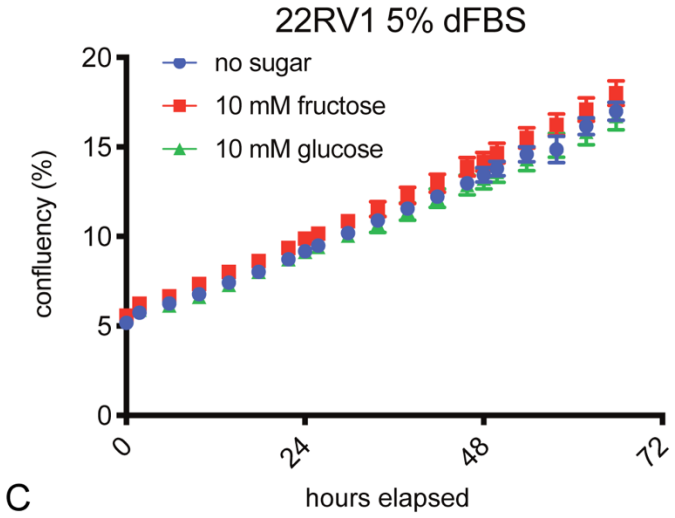

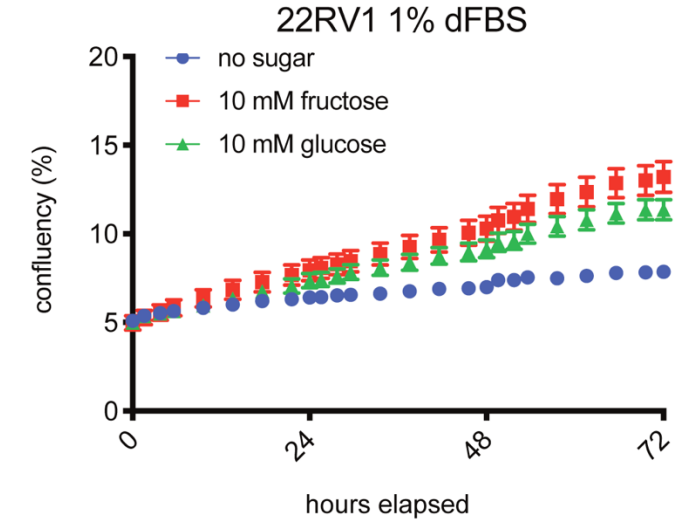

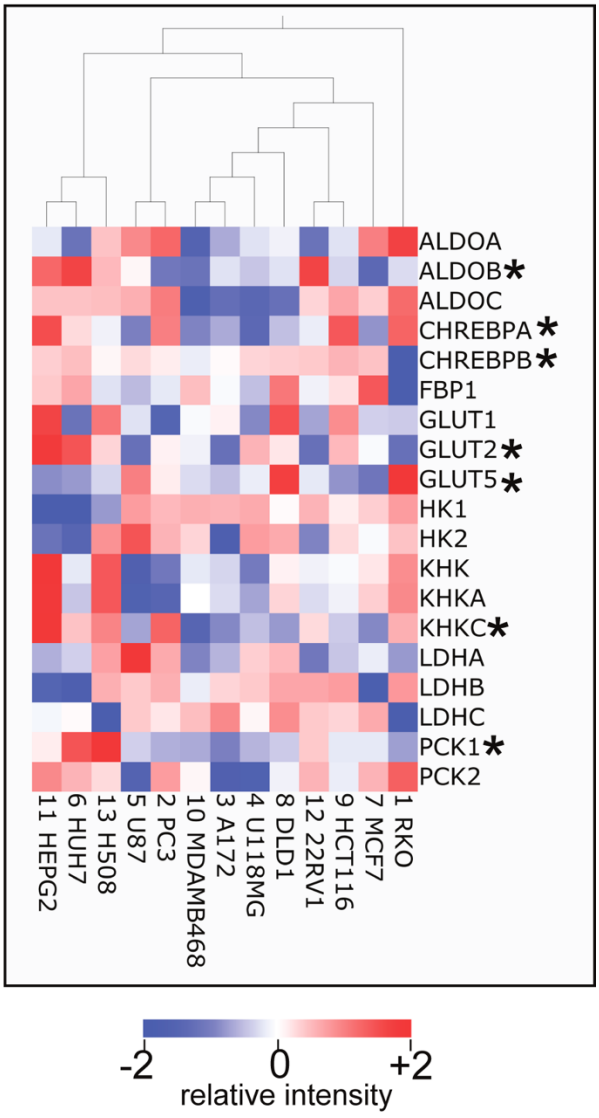

Supplemental Figure 2

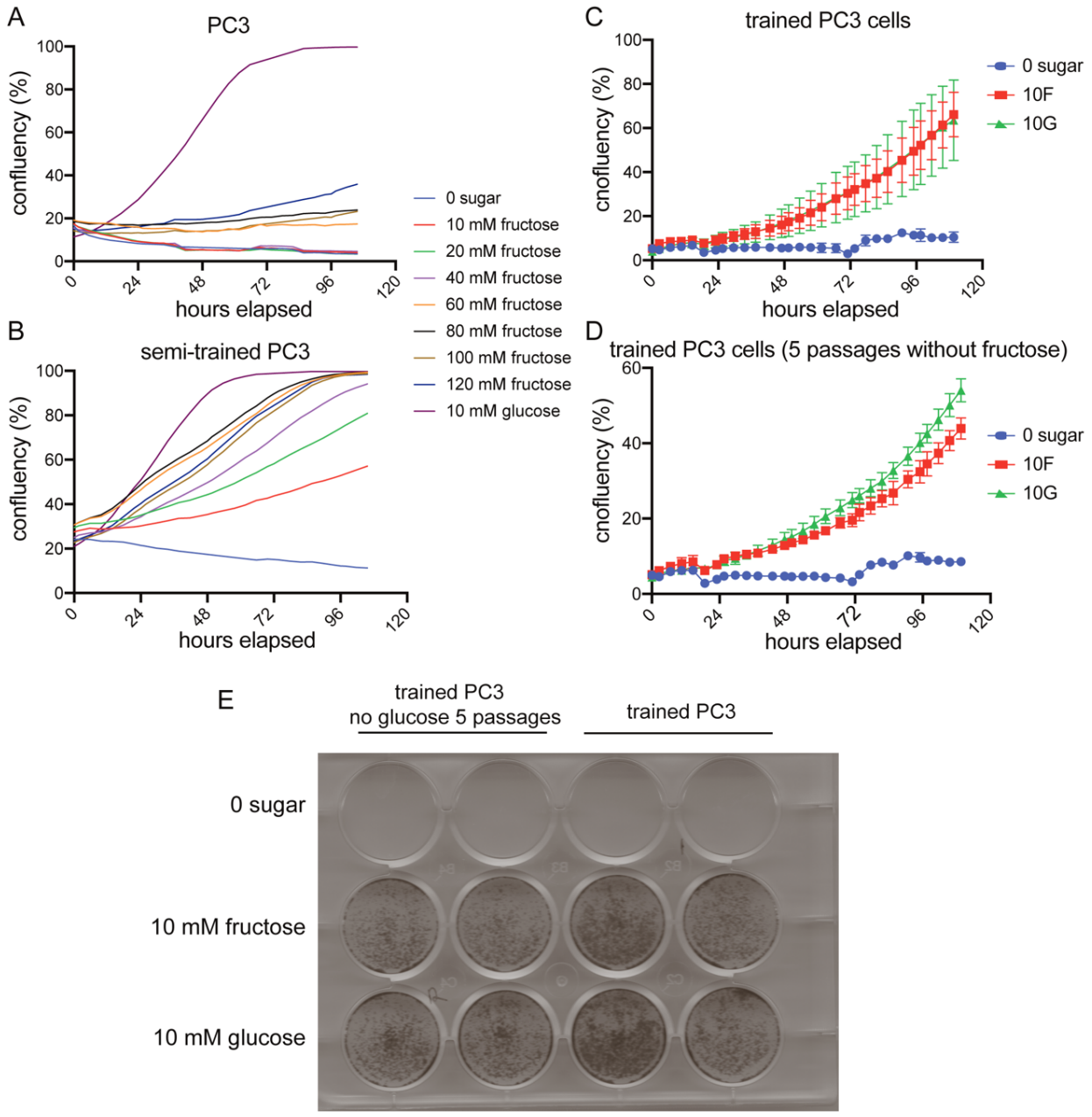

Supplemental Figure 3

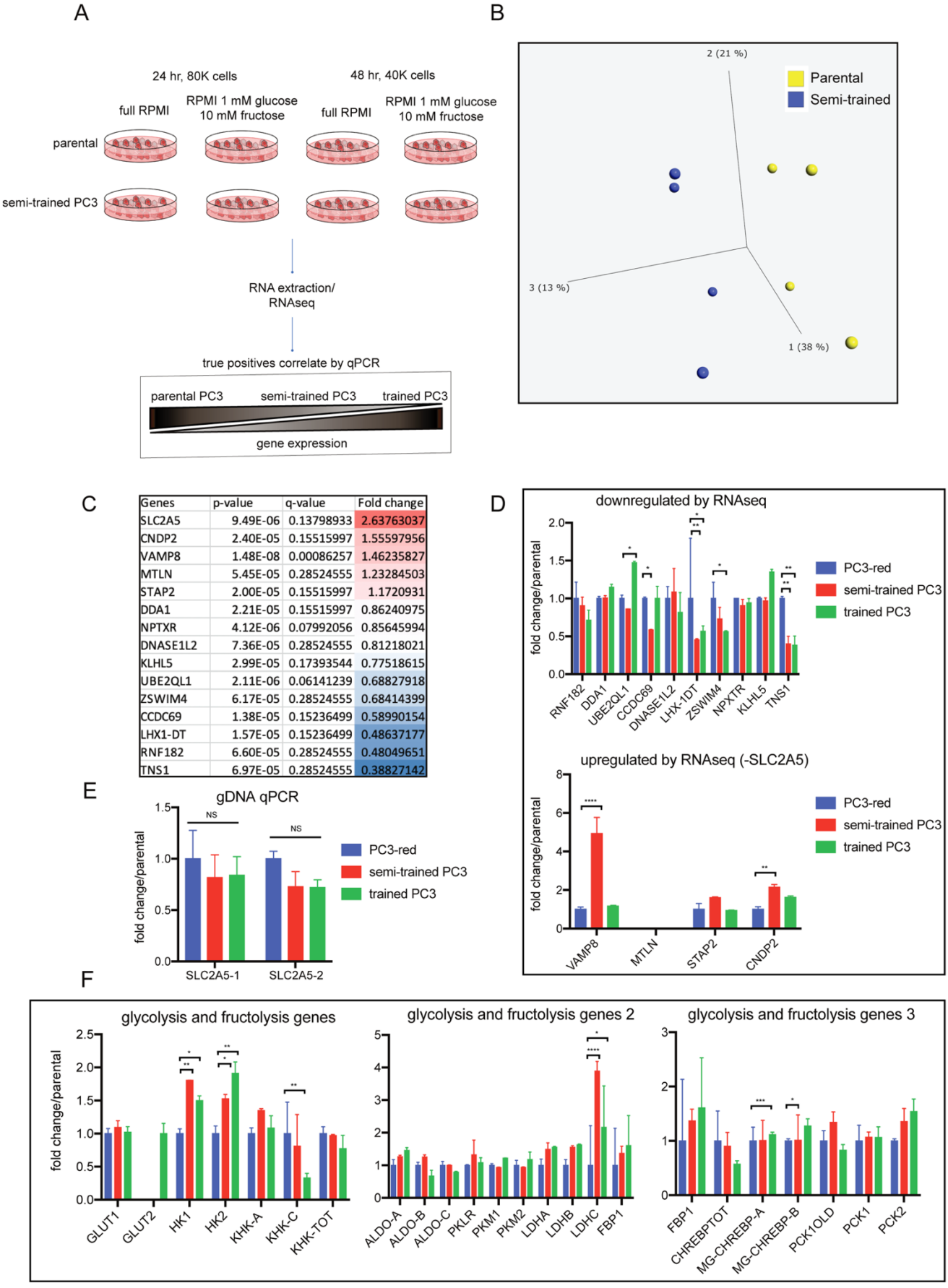

Supplemental Figure 4

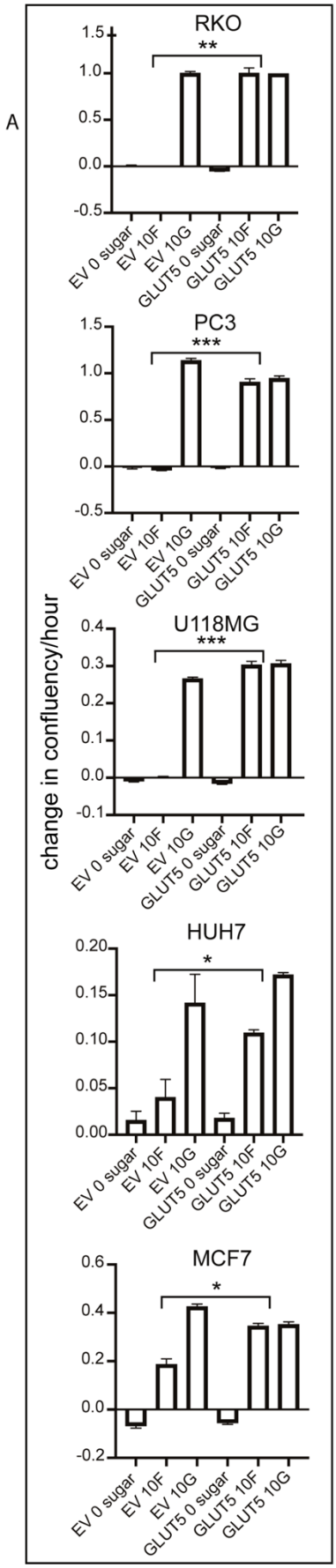

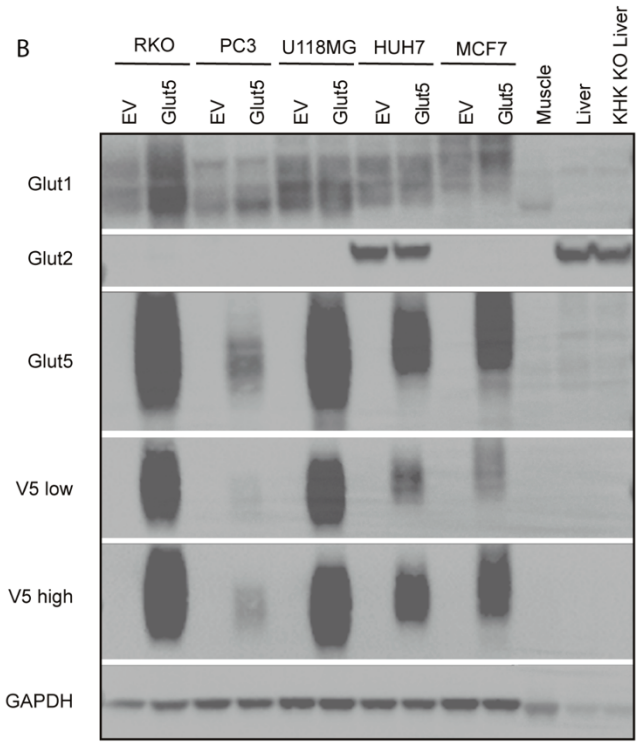

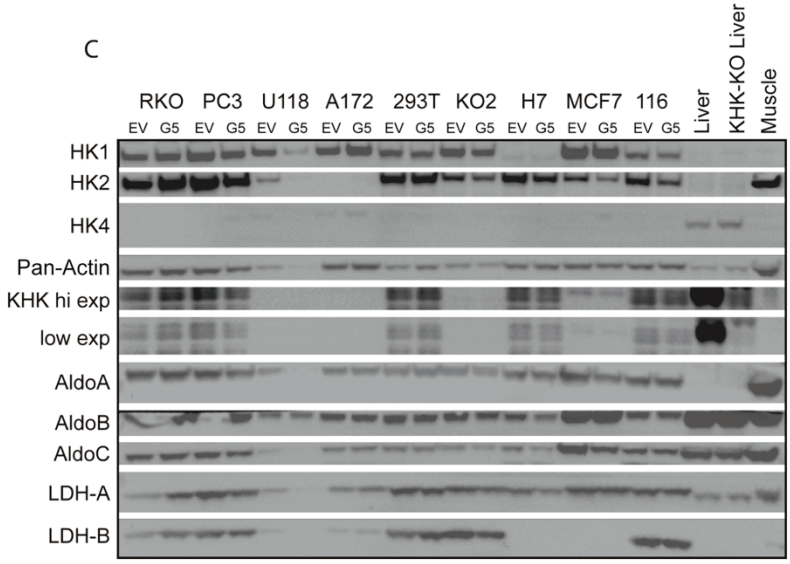

Supplemental Figure 5

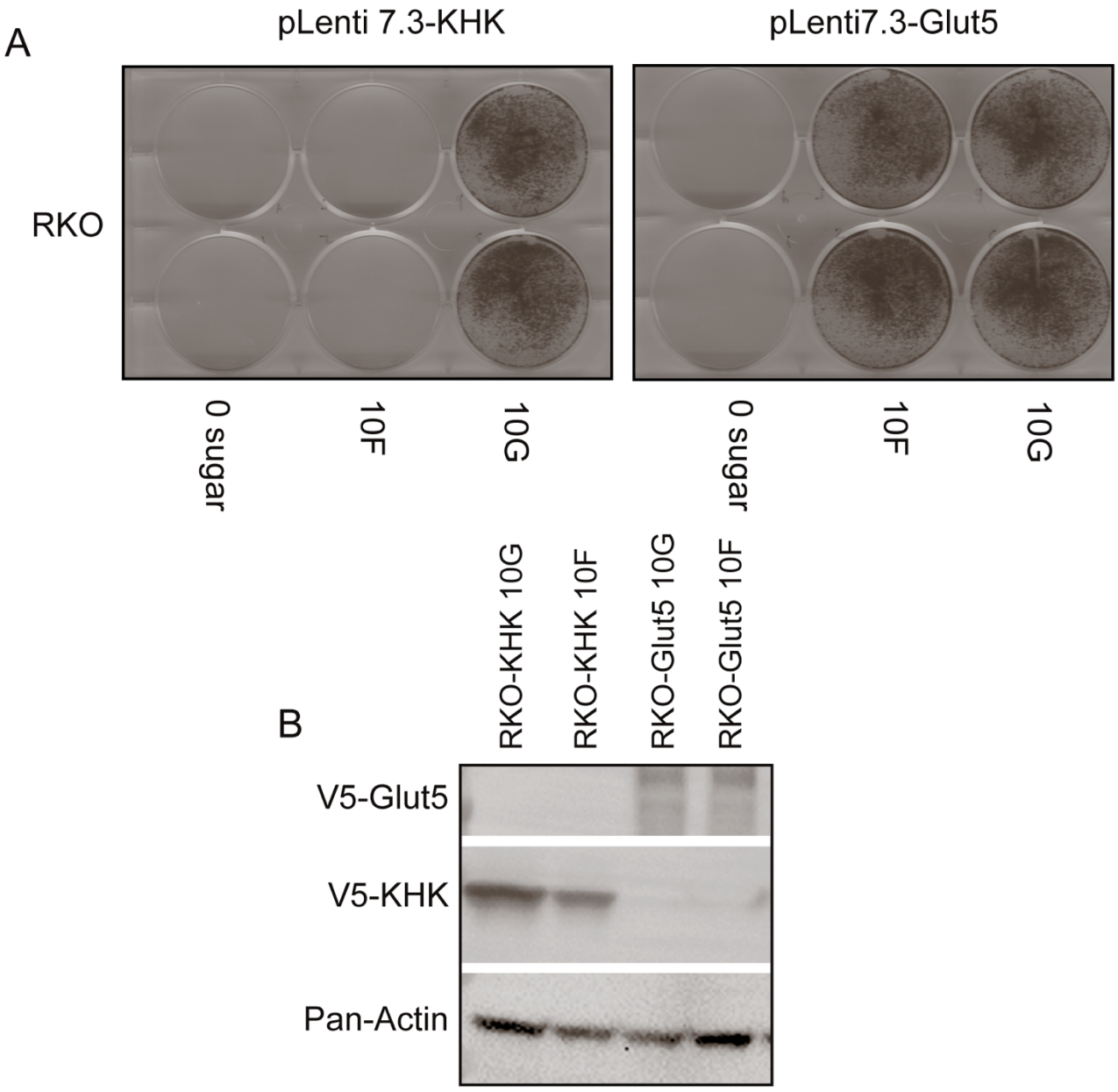

Supplemental Figure 6

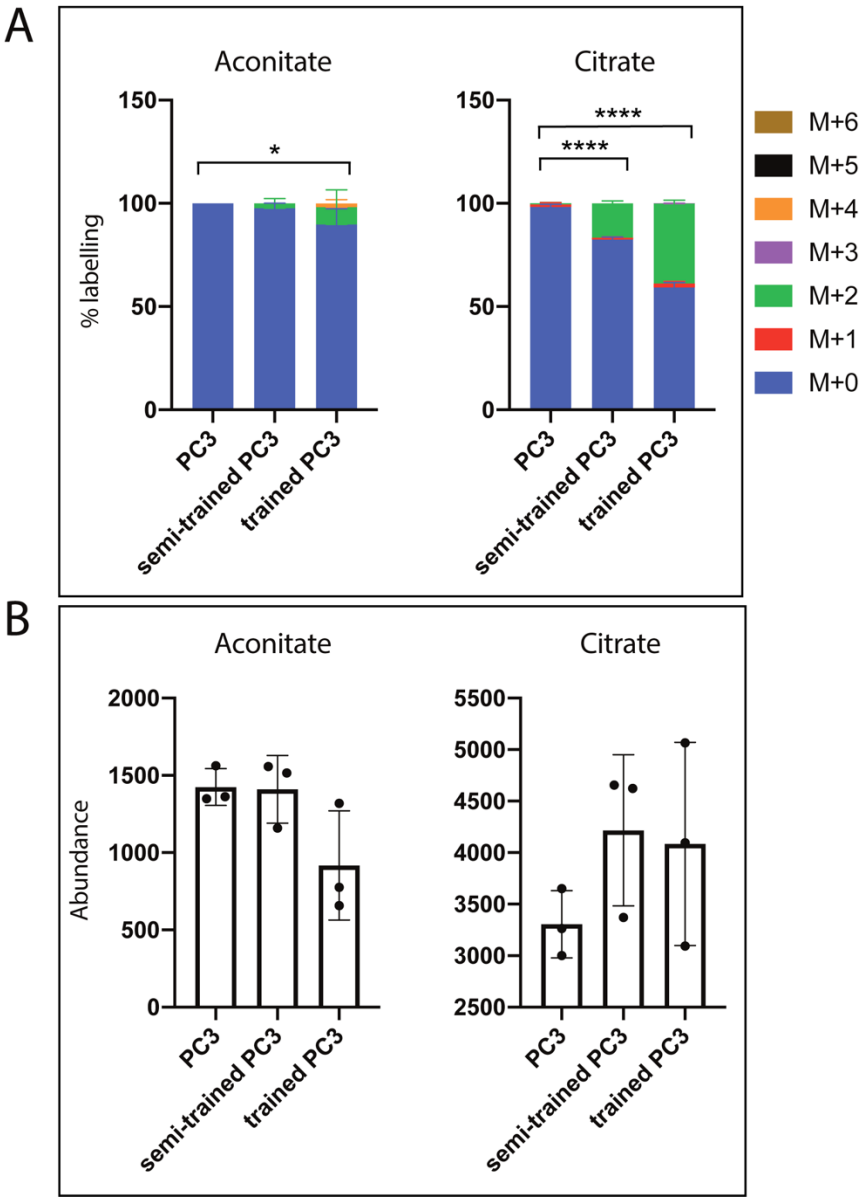

Supplemental Figure 7

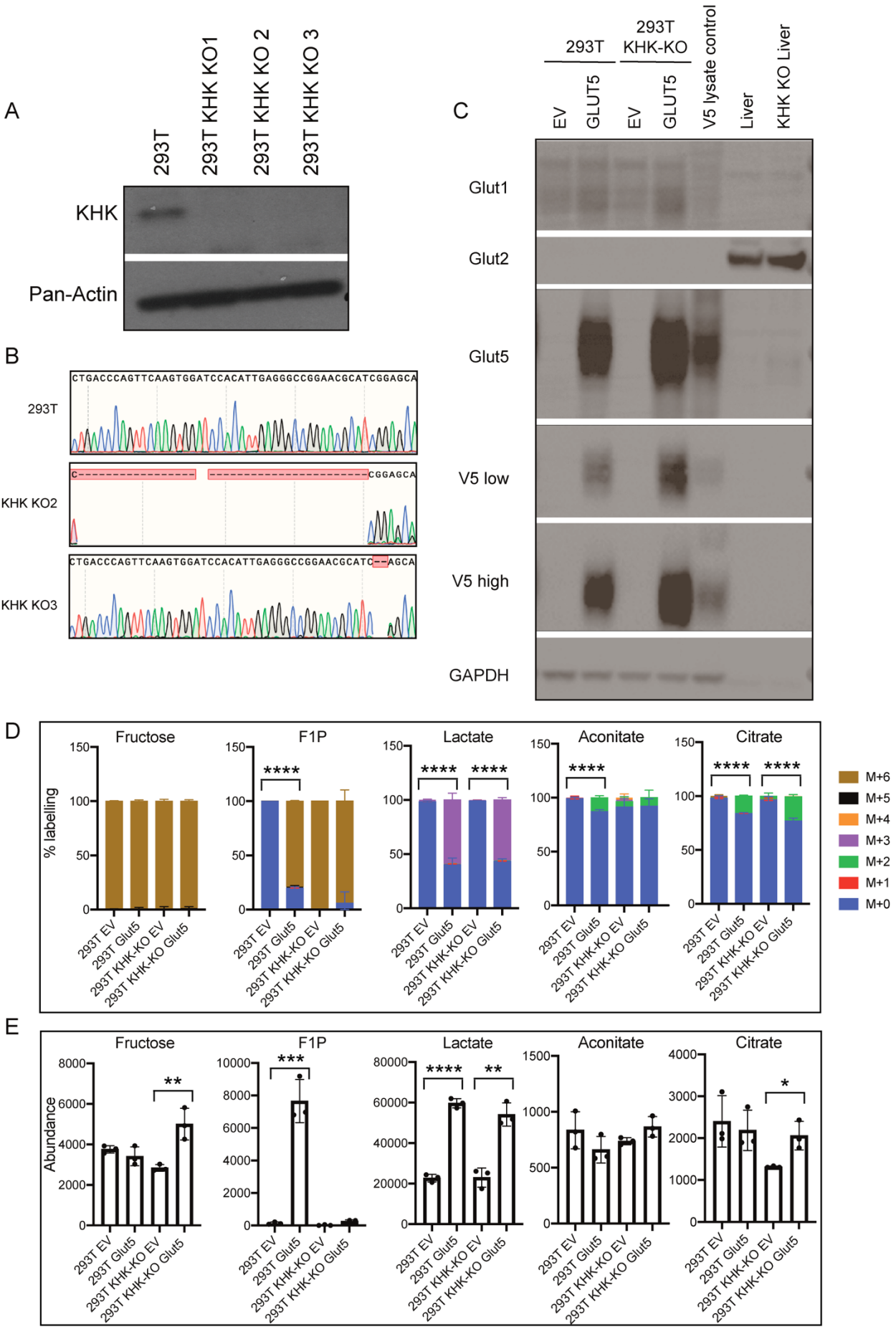
A
293T
293T KHK KO1
293T KHK KO 2
293T KHK KO 3
KHK
Pan-Actin
B
293T
CTGACCCAGTTCAAGTGGATCCACATTGAGGGCCGGAACGCATCGGAGCA
293T KHK KO2
C----------CGGAGCA
293T KHK KO3
CTGACCCAGTTCAAGTGGATCCACATTGAGGGCCGGAACGCATC--AGCA
C
293T
293T KHK-KO
EV
GLUT5
EV
GLUT5
V5 lysate control
Liver
KHK KO Liver
Glut1
Glut2
Glut5
V5 low
V5 high
GAPDH
D
Fructose
F1P
Lactate
Aconitate
Citrate
% labeling
150
100
50
0
****
293T EV
293T Glut5
293T KHK-KO EV
293T KHK-KO Glut5
M+6
M+5
M+4
M+3
M+2
M+1
M+0
E
Fructose
F1P
Lactate
Aconitate
Citrate
Abundance
8000
6000
4000
2000
0
10000
80000
60000
40000
20000
1500
1000
500
4000
3000
2000
1000
**
***
****
*

Supplemental Figure 8

Supplemental Figure 1: Cell growth in fructose is heterogeneous.

(A) Cells were seeded at 40,000-50,000 cells/well into 6-well plates or at 20,000-30,000 cells/well into 12-well plates. They were then cultured in media containing no sugar, 10 mM fructose, or 10 mM glucose and cell density (% confluency) was monitored over 72-96 hours using live cell imaging (n = 2 per media condition).
(B) Cells from (A) were grown in media containing 10 mM fructose or 10 mM glucose for 72-96 hours. They were then fixed and stained with crystal violet solution (n = 2 per condition).

Supplemental Figure 2: Gene expression does not determine the fructolytic index

(A) Example calculation of the fructolytic index. MCF7 cells were plated in a 12-well plate at 20,000 cells/well and were then cultured in media containing no sugar, 10 mM fructose or 10 mM glucose. The slopes of each condition are noted as “a, b, c” (n = 2 per condition).
(B) 22RV1 were seeded at 1,000 cells/well into a 96-well plate and cultured in media containing no sugar, 10 mM fructose, or 10 mM glucose and cell density (% confluency) was monitored over 72-96 hours using live cell imaging (n = 2 per condition).
(C) 22RV1 were seeded at 1,000 cells/well into a 96-well plate and cultured in media containing no sugar, 10 mM fructose, or 10 mM glucose and cell density (% confluency) was monitored over 72-96 hours using live cell imaging (n = 2 per condition).
(D) Normalized expression of the indicated genes for each cell line shown as a heatmap with hierarchical clustering performed on the cell lines. Relative fructolytic index is denoted next to sample names (n = 2 per gene per sample). * denotes $C_t > 30$.

Supplemental Figure 3: Cells can stably utilize fructose for proliferation

(A) PC3 cells were seeded at 1,000 cells/well in a 96-well plate and cultured in media containing the specified concentrations of sugars and cell density (% confluency) was monitored over 72-96 hours using live cell imaging (n = 1 per condition).
(B) Semi-trained PC3 cells were seeded at 1,000 cells/well in a 96-well plate and cultured in media containing the specified concentrations of sugars and cell density (% confluency) was monitored over 72-96 hours using live cell imaging (n = 1 per condition).
(C) Trained PC3 cells were seeded at 20,000 cells/well into a 12-well plate and cultured in media containing no sugar, 10 mM fructose, or 10 mM glucose and cell density (% confluency) was monitored over 120 hours using live cell imaging (n = 2 per condition).
(D) Trained PC3 cells were seeded at 20,000 cells/well into a 12-well plate and cultured in the absence of fructose for 5 passages. These cells were then seeded into a 12-well plate and cultured in media containing no sugar, 10 mM, or 10 mM glucose and cell density (% confluency) was monitored over 72-96 hours using live cell imaging (n = 2 per condition).
(E) Cells from (C) and (D) were grown in media containing no sugar, 10 mM fructose, or 10 mM glucose for 5 days. They were then fixed and stained with crystal violet (n = 2 per condition).

Supplemental Figure 4: *SLC2A5* copy number, validated RNA-seq transcripts (excluding *SLC2A5*), and selected metabolic enzyme transcripts do not correlate with fructolytic ability.

(A) Schematic of RNA-seq sample conditions. Parental and semi-trained PC3 cells were grown at 2 cell densities (80,000 and 40,000 cells/well) and 2 time points (24 or 48 hours) in media containing 11 mM glucose or 1 mM glucose plus 10 mM fructose. RNA was extracted and RNA-seq was performed. Fructose metabolism-related trends between parental and semi-trained PC3 were hypothesized to be exaggerated in trained PC3 cells.

(B) Principle Components Analysis (PCA) of PC3 and semi-trained PC3 from data generated in (A). Fragments per kilobase per million reads mapped (FPKM) was $\log_2$ transformed prior to performing PCA.
(C) Table of differential gene expression (q = 0.4, >1.1 $\log_2$ fold change) between PC3 and semi-trained PC3 with associated p-value, q-value, and fold changes.
(D) Relative expression of differentially expressed transcripts (excluding *SLC2A5*) from RNA-seq. Semi-trained PC3 and trained PC3 cells were compared to the parental PC3 line. Relative *SLC2A5* expression is located in Figure 3B (n = 2 per gene per cell line). Two-way ANOVA with Fisher's LDS test.
(E) Copy number of *SLC2A5* determined by intra-exonic qPCR on genomic *SLC2A5* in PC3-red, semi-trained PC3, and trained PC3 cells (n = 2 per primer set per cell line). Two-way ANOVA with Fisher's LDS test.
(F) Normalized gene expression of the indicated metabolism-related genes in PC3-red, semi-trained PC3, and trained PC3 cells (n = 2 per gene per cell line). Two-way ANOVA with Fisher's LDS test. *P < 0.05, **P< 0.01, and ****P < 0.0001. NS = "not significant."

Supplemental Figure 5: Selected metabolism genes are not changed with GLUT5 overexpression

(A) GLUT5 or an empty vector (EV) were overexpressed in the indicated cell lines. The cells were plated at 20,000-30,000 cells/well and then cultured in media containing no sugar, 10 mM fructose, or 10 mM glucose. Two-tailed unpaired t test were used to determine significance between the cell line overexpressing EV and GLUT5 in the 10 mM fructose condition. *P < 0.05, **P< 0.01, ***P < 0.001, and ****P < 0.0001.
(B) Immunoblot of the indicated proteins using lysates from the indicated panel of cells. Murine muscle, liver, and *Khk* $^{-/-}$ liver were used as controls.
(C) Immunoblot of the indicated proteins using cell lines overexpressing GLUT5 or EV. Murine liver, *Khk* $^{-/-}$ liver, and muscle were used as controls.

Supplemental Figure 6: KHK overexpression does not rescue the ability to proliferate in fructose

(A) KHK-A or GLUT5 were overexpressed in RKO cells. 50,000 cells were then plated into 6-well plates and cultured in media containing no sugar, 10 mM fructose, or 10 mM glucose. After 7 days, cells were fixed and stained with crystal violet solution (n = 2).
(B) Immunoblot of V5 and Pan-Actin using lysates from the cells in (A) after being cultured for 4 hours in media containing 10 mM fructose or 10 mM glucose.

Supplemental Figure 7: Trained PC3 have increased fructose flux into the TCA cycle

(A) Percent of heavy isotope (^{13}C) incorporation into aconitate and citrate as detected by LC/MS from polar extracts of PC3, semi-trained PC3, and trained PC3 (n = 2-3). The isotopic labelling is indicated by M+# designation indicated in the legend where the # represents the amount of [^{12}C] replaced by [^{13}C]. Two-tailed unpaired t tests of the M+2 isotope were used between parental and trained cells. *P < 0.05, **P< 0.01, and ****P < 0.0001.
(B) Total abundance of aconitate and citrate as detected by LC/MS from polar extracts of PC3, semi-trained PC3, and trained PC3 cells (n = 2-3). Two-tailed unpaired t tests were used between parental and trained cells. *P < 0.05, **P< 0.01, ***P < 0.001, and ****P < 0.0001.

Supplemental Figure 8: Trained PC3 have increased fructose flux into the TCA cycle

(A) Immunoblot of KHK and Pan-Actin using lysates from parental and *KHK* $^{-/-}$ 293T cells (293T-KO#).

(B) Sanger sequencing results of parental 293T, 293T-KO2, and 293T-KO3. 293T-KO2 was subsequently used below (D-G) and is referred to as 293T *KHK* $^{-/-}$.
(C) Immunoblot of the indicated proteins using lysates from parental 293T or 293T *KHK* $^{-/-}$. The control GLUT5-V5 lysate was derived from several cell lines that had previously verified expression of GLUT5-V5. Murine liver and *Khk* $^{-/-}$ liver were also used as controls.
(D) Percent of heavy isotope (^{13}C) incorporation into fructose, fructose-1-phosphate (F1P), lactate, aconitate, and citrate, as detected by LC/MS from polar extracts of 293T and 293T *KHK* $^{-/-}$ cells overexpressing EV or GLUT5 (n = 2-3). The isotopic labelling is indicated by M+# designation indicated in the legend where the # represents the amount of [^{12}C] replaced by [^{13}C]. Two-tailed unpaired t tests were used between 293T or 293T *KHK* $^{-/-}$ expressing EV and GLUT5 (M+3 for lactate, M+6 for fructose/F1P, M+2 for aconitate/citrate). *P < 0.05, **P< 0.01, ***P < 0.001, and ****P < 0.0001.
(E) Total abundance of fructose, F1P, lactate, aconitate, and citrate in 293T or 293T *KHK* $^{-/-}$ cells with EV or GLUT5 overexpression. (n = 3 per sample). Two-tailed unpaired t tests were used between 293T or 293T *KHK* $^{-/-}$ expressing EV and GLUT5. *P < 0.05, **P< 0.01, ***P < 0.001, and ****P < 0.0001.

Supplemental Video 1: Trained PC3 cells outcompete parental PC3 cells in fructose media. 20,000 PC3-red and 20,000 trained PC3 cells were seeded in a 6-well dish containing 10 mM fructose. Cells were monitored with live cell imaging for 4 days.

Supplemental Video 2: Trained PC3 cells grow at the same rate as parental PC3 cells in glucose media. 20,000 PC3-red and 20,000 trained PC3 cells were seeded in a 6-well dish containing 10 mM glucose. Cells were monitored with live cell imaging for 4 days.

Name	Origin	Grade (1-4)	Fructolytic index	Age of sampling	Sex	Metastasis/Primary	Key Genomic Alterations
RKO	Colon	3-4	-0.015 ± 0.001	Unspecified	Unspecified	Primary	B2M p.R117*; BRAF p.V600E; BRCA1 p.D435Y; BRCA2 p.Q1782fs; IDH1 p.N213fs; IDH2 p.G190D; KEAP1 p.G350S; KIT p.L641P; MYC p.A337V; PIK3CA p.H1047R
PC3	Prostate	4	0.005 ± 0.009	62	Male	Metastasis (bone)	HIF1A p.Y659N; PTEN p.R55fs; TP53 p.A138s
A172	Brain	4	0.046 ± 0.033	53	Male	Primary	CDKN2A p.0?; PTEN p.R55fs*; RB1 p.V852L
U118MG	Brain	4	0.108 ± 0.092	47	Male	Primary	CDKN2A p.0?; MTOR p.L1129P; PTEN p.0?; TP53 p.R213Q
U87	Brain	4	0.132 ± 0.057	unspecified	Male	Primary	CDKN2A p.0?; PTEN p.0?
Huh7	Liver	1-2	0.311 ± 0.07	57	Male	Primary	TP53 p.Y220C
MCF7	Breast	N/A	0.334 ± 0.044	69	Female	Metastasis (pleura)	CDKN2A p.0?; PIK3CA p.E545K
DLD1	Colon	3-4	0.572 ± 0.041	Adult	Male	Primary	APC p.R26Q; B2M p.T517M; CDKN2A p.A290D; FGFR1 p.T322P; HIF1A p.S87C; IDH1 p.A1096T; KIT p.T751I; PIK3CA p.R628Q; PIK3CB p.P312L; PIK3R1 p.D68V; TGFBR2 p.A648S
HCT116	Colon	1-2	0.602 ± 0.088	48	Male	Primary	ATM p.A1127V; CDKN2A p.R24fs; CTNNB1 p.S45del; IDH1 p.S261L; KIT p.A115T; KRAS p.G13D; PIK3CA p.H1047R
MDA-MB-468	Breast	N/A	0.846 ± 0.045	51	Female	Metastasis (pleura)	BRCA2 p.M965I; PTEN p.0?; RB1 p.0?; SMAD4 p.0?; TP53 p.R273H
HepG2	Liver	3-4	0.916 ± 0.032	15	Male	Primary	ATM p.V2906I; NRAS p.Q61L

22RV1	Prostate	N/A	0.917 ± 0.034	Adult	Male	Primary	ATM p.K1101E; BRAF p.L597R; KEAP1 p.T314M; MTOR p.V420I; PIK3CA p.Q546R; STK11 p.E407D; TP53 p.P72fs; TSC1 p.0
H508	Cecum	N/A	1.057 ± 0.132	55	Male	Metastasis (abdominal wall)	BRAF p.G596R; PIK3CA p.E545K; TP53 p.R273H

Supplemental Table 1: Clinical and genomic data of profiled cell lines in order of fructolytic index. Related to Figure

	RKO	PC3	A172	U118MG	U87	HUH7	MCF7	DLD1	HCT116	MDAMB468	HEPG2	22RV1	H508
GLUT1	0.000870054	0.000296415	0.00148508	0.000551812	0.001051314	0.000408277	0.000913327	0.006032212	0.003249921	0.001247167	0.00699753	0.000678268	0.0040315
GLUT2	#VALUE!	1.1566E-07	#VALUE!	2.53158E-06	#VALUE!	0.001361257	3.20712E-08	1.7622E-07	1.99396E-06	1.91679E-08	0.026057665	#VALUE!	4.15077E-07
GLUT5	5.77833E-06	1.31387E-06	8.05739E-07	1.01778E-06	2.48831E-06	6.41231E-07	4.85206E-07	4.4225E-06	6.28511E-07	9.18042E-07	5.94991E-07	9.79416E-07	8.87771E-07
CHREBPA	4.55839E-06	3.98933E-06	1.69842E-06	1.14528E-06	1.41341E-06	2.71863E-06	1.53718E-06	1.81332E-06	4.88103E-06	1.44338E-06	5.19476E-06	2.18064E-06	2.23202E-06
CHREBPB	#VALUE!	3.22789E-07	2.24523E-07	4.92512E-07	4.5399E-07	7.74116E-07	7.04798E-07	5.87705E-07	9.9578E-07	1.15619E-07	5.37022E-07	6.26007E-07	2.36849E-07
KHKA	0.000365813	4.56619E-05	0.000129147	8.93351E-05	3.92475E-05	0.000111581	0.000224093	0.000220427	0.000148782	0.000166365	0.000867399	0.000126853	0.000563429
KHKC	4.19276E-06	1.06743E-05	5.32595E-07	9.3522E-07	6.84897E-07	3.38952E-06	5.23117E-07	6.14528E-07	1.0576E-06	2.45237E-07	2.59414E-05	2.68403E-06	6.82605E-06
KHK	0.000258858	0.000199716	6.99918E-05	4.62883E-05	2.54089E-05	8.43124E-05	0.000128439	0.000167805	0.000156771	7.46697E-05	0.000595922	0.00039884	0.000369952
KHKex4	0.000184287	3.18406E-05	6.18385E-05	3.285E-05	1.95855E-05	7.01308E-05	0.000101794	9.46672E-05	8.21934E-05	6.9766E-05	0.000509797	7.48202E-05	0.000290453
ALDOA	0.057368024	0.048190581	0.024113807	0.02816367	0.043155924	0.019998123	0.0442225	0.029400564	0.028037436	0.017478549	0.02867551	0.020083609	0.036160359
ALDOB	1.07897E-05	4.83846E-06	1.11625E-05	9.04863E-06	1.53538E-05	7.39414E-05	3.66709E-06	1.10822E-05	1.01136E-05	4.44175E-06	4.86471E-05	7.22905E-05	2.42068E-05
ALDOC	0.007183357	0.005095396	4.32817E-05	2.98214E-05	0.002173804	0.0014671	0.00129923	4.57446E-05	0.002411642	1.64225E-05	0.001522545	0.001198757	0.001623555
FBP1	#VALUE!	1.2562E-06	2.59324E-06	2.95207E-07	2.74772E-07	7.30743E-05	0.002361403	0.000491147	8.87533E-06	3.08101E-05	2.125E-05	1.68124E-06	9.24127E-07
HK1	0.003822233	0.002164596	0.002414495	0.002913511	0.003811259	5.38347E-06	0.001461697	0.000717597	0.000986378	0.002554725	5.21606E-06	0.002397574	0.000106551
HK2	6.6625E-05	7.06756E-05	2.29878E-05	7.80997E-05	0.000108489	2.67465E-05	5.27755E-05	7.3545E-05	6.17584E-05	6.27094E-05	3.05105E-05	3.45278E-05	8.02114E-05
LDHA	0.028846076	0.048680201	0.031116111	0.043827278	0.10424297	0.033755351	0.035953894	0.046762747	0.032697751	0.027144358	0.03091596	0.025838144	0.050057685
LDHB	0.062043812	0.034737264	0.015591724	0.020270069	0.019983681	5.28398E-05	4.16462E-05	0.043397778	0.052799242	0.00406883	0.000109673	0.041478224	0.034837971
LDHC	#VALUE!	2.08502E-06	8.65433E-05	1.0577E-06	6.09923E-06	9.9517E-07	2.19608E-05	7.63203E-05	3.86669E-06	8.70338E-06	5.10049E-07	6.62672E-06	#VALUE!
PCK1	8.40558E-07	1.01262E-06	5.86034E-07	1.05634E-06	1.46186E-06	2.17589E-05	1.85654E-06	1.3425E-06	1.78065E-06	9.46474E-07	3.19806E-06	4.49606E-06	0.000121748
PCK2	0.001848486	0.000963597	5.67702E-05	5.99824E-05	6.47193E-05	0.000744889	0.000746335	0.000341378	0.000324575	0.000421063	0.001161182	0.000738792	0.000536503
GAPDH	0.237135156	0.204108001	0.075379783	0.200343033	0.236108266	0.170998396	0.17150057	0.183242265	0.17220854	0.130239052	0.155951196	0.189088439	0.118233405
ACTIN	0.048646193	0.038275342	0.216412038	0.107165607	0.09501038	0.086943139	0.1072036	0.091008917	0.05778167	0.122248019	0.086851578	0.05930823	0.104302624
H18S	86.80487617	128.2576138	61.33956049	46.68407272	44.67535868	67.2920604	54.77110034	59.96738947	100.5328286	62.80828605	74.1548622	89.59038895	81.2290131
average	1	1	1	1	1	1	1	1	1	1	1	1	1

Supplemental Table 2: qPCR data for each cell line using primers from Supplemental File 1. (n = 2 per gene per sample, 2^dC$_t$ values shown). Related to Figure 1

qPCR screening primers	Forward	Reverse
SLC2A1	AACTCTTCAGCCAGGGTCCAC	CACAGTGAAGATGATGAAGAC
SLC2A2	CATGCTCTGGTCCCTGTCTGTATC	AACCCCATCAAGAGAGCTCCAACT
SLC2A5	CCAGAGCAAGCATGGAGCAAC	AGGATGACCCAAAGGCAGCTA
HK1	GCTCTCCGATGAAACTCTCATAG	GGACCTTACGAATGTTGGCAA
HK2	CGGCCGTGCTACAATAGG	CTCGGGATCATGTGAGGG
KHK	AATGCCTCCGTCATCTTCAGCC	ACCTGCTCTCACACGATGCCAT
KHK-A	GCCCCCTGTGCCTTCAT	CGGAGCCTGTGGTCTGAAA
KHK-C	GCCCCCTGTGCCTTCAT	CCACCTGAGACACGTCCAC
ALDO-A	ATGCCCTACCAATATCCAGCA	GCTCCCAGTGGACTCATCTG
ALDO-B	TGTCTGGTGGCATGAGTGAAG	GGCCCGTCCATAAGAGAAACTT
ALDO-C	TGCTGATGACCGTGTGAAAAA	CGGACGAAGGGAACACCAT
LDHA	AGCCCGATTCCGTTACCT	CACCAGCAACATTCATTCCA
LDHB	GGACAAGTTGGTATGGCGTGTG	AAGCTCCCATGCTGCAGATCCA
LDHC	CCTCTTGGGCTATTGGACTG	GCCTCCTCCTCAGAATTCAA
H18S	CGCCGCTAGAGGTGAAATTC	TTGGCAAATGCTTTCGCTC
GAPDH	TGGGTGTGAACCATGAGAAG	GCTAAGCAGTTGGTGGTGC
RPLP0	GGCACCATTGAAATCCTGAG	GAAGGGGGAGATGTTGAGC
ACTB	ATGAAGATCAAGATCATTGCTCCTC	ACATCTGCTGGAAGGTGGACA
FBP1	ACATCGATTGCCTTGTGTCC	CCACCAAAATGAACTCCCCG
CHREBPA	CGACACTCACCCACCTCTTC	TTGTTCAGCCGGATCTTGTC
CHREBPB	TCTGCAGATCGCGTGGAG	CTTGTCCCGGCATAGCAAC
CRISPR-cas9 primers	**Forward**	**Reverse**
459-KHK-KO2	TCACCTGCTCCGATGCGTTC	GAACGCATCGGAGCAGGTGA
459-KHK-KO3	GGGCCGGAACGCATCGGAGC	GCTCCGATGCGTTCCGGCCC
gDNA primers	**Forward**	**Reverse**
SLC2A5-1	ATCTACTACTACGCGGACCAGAT	TACTGCACGTGCTCCTCCG
SLC2A5-2	CAGGAGGATGAGGCAGAGAA	AGCGCATCCGGAACAGCTT
B2M	TGCTGTCTCCATGTTTGATGTATCT	TCTCTGCTCCCCACCTCTAAGT

Supplemental Table 3: qPCR primers for selected metabolic genes, CRISPR-cas9 primers, and qPCR primers for gDNA. Related to Figure 1, 4 and Supplemental Figure 4, 8.

RNAseq validation primers	Forward	Reverse
RNF182	TGCCCGTGTGAGCTAGCA	AGAACGGAGATATCCATGGTGAA
DDA1	GCCCTCAGTCTACCTGCCTA	TCCTGGTCTCTCTTCTTGGC
UBE2QL1	GCAGCCAGCCTGGTCAA	TCAGCTTCCTTGCGACTGAA
CCDC69	CTGCAAACCCCCGAAAA	CTAATTCATGGGGCTCTGGTCT
DNASE1L2	CTTCGGTGACAGCAAAGTGT	ACCAGCGCGAGGTCATA
LHX1-DT	GGAGACCGCGTTTAGAGGAT	GTCATTCTGGAACCGGAGCA
ZSWIM4	GCTGGGCCTTCGAGCA	CTGCGTGGAAACGACCAAAA
NPTXR	ACTCGCCTGCGCTCATT	GCTGAGAGGTTCACACGGG
KLHL5	GGCTGGATAGACCAGAAGTGG	GGCTCCATAGTATGACAGGATGATA
TNS1	ACTCCAGAGGAGGAGCCATTGA	TGTGGCTTCTGGAGACTGGTTC
VAMP8	CATCTCCGCAACAAGACAGA	GACCCTCCTGGCACACATTT
MTLN	CTGGAGGATGGTGGTCCTAAA	AAGCTCTTCACCGCTCTGTATTT
STAP2	CCAAGCCTAAGGGTGTCCTG	CAGGCCTGCCCAGAACTT
CNDP2	TTGCTGATGGGCTCTTTGGT	TCGATGTCGTCGTACAGCTTGT
SLC2A5-1	CCAGAGCAAGCATGGAGCAAC	AGGATGACCCAAAGGCAGCTA
SLC2A5-2	GGCTTCTCCATCTGCCTCATAG	GATGACACAGACGATGCTGATGT

Supplemental Table 4: qPCR primers for RNA-seq hits, related to Figure 3 and Supplemental Figure 4